
Article:
Tian, Y., Gao, X., Liu, W. orcid.org/0000-0003-2968-2888 et al. (3 more authors) (2022) Localization of mixed far-field and near-field incoherently distributed sources using two-stage RARE estimator. IEEE Transactions on Aerospace and Electronic Systems. ISSN 0018-9251

https://doi.org/10.1109/taes.2022.3201069

Localization of Mixed Far-field and Near-field Incoherently Distributed Sources Using Two-stage RARE Estimator

Ye Tian, *Member, IEEE*, Xinyu Gao, Wei Liu, *Senior Member, IEEE*, Hua Chen, *Member, IEEE*, Gang Wang, *Senior Member, IEEE*, and Yunbai Qin

***Abstract*—In this paper, a mixed source localization method utilizing a two-stage rank-reduction (RARE) estimator is investigated. Different from the existing methods, the proposed one is built on the incoherently distributed (ID) source model, which is more appropriate for multipath and fast time-varying channels. Firstly, a general array manifold (GAM) model is established, where nominal DOAs and nominal ranges are extracted from the initial array manifold. By exploiting the shift invariance property of the far-field (FF) GAM and combining virtual source enumeration result, nominal FF DOA estimation is achieved by a one-dimensional (1-D) RARE spectral search. Secondly, the oblique projection operation is adopted to separate near-field (NF) sources, and the nominal DOA and range parameters of NF sources are subsequently obtained by jointly utilizing the manifold separation technique (MST) and another two 1-D spectral searches. With the estimated nominal DOA and range parameters, the angular spread and range spread are then successfully estimated. Moreover, the Cramér-Rao bound (CRB) for the considered case is also derived. Simulation results are presented to validate the effectiveness of the proposed method.**

***Index Terms*—Incoherently distributed (ID) sources, far-field, near-field, general array manifold, rank-reduction estimator.**

I. Introduction

SOURCE localization using antenna array is one of important issues in signal processing, and it has been widely applied in civilian and military fields, such as wireless communications, seismic exploration, radar, sonar, aerospace and electronic surveillance [1]-[3]. According to the aperture size of antenna array and the location of the detected target (DT), source localization is mainly divided into two types: far-field (FF) source localization and near-field (NF) source localization. For FF sources, the signal wavefront is only characterized by direction of arrival (DOA) information. In contrast, when a source is located closely enough to the array, it is classified as an NF one, and the wavefront must be characterized by both the DOA and range information [4]. So far, a large number of localization methods for pure FF and pure NF sources have been proposed, such as the subspace based methods [5]-[7], the sparse reconstruction based methods [8]-[10] and the deep learning based methods [11], [12].

However, in some practical systems (such as massive multiple-input multiple-output (MIMO) systems) equipped with large-scale antenna arrays, the array aperture is normally much larger than the traditional case. As a result, the distance between DT and antenna array is likely to be shorter than the Rayleigh distance [13], and the received signals by the antenna array may be considered as a mixture of FF and NF sources [14]. In this case, the performance of the methods developed for pure FF/NF sources could degrade substantially. Recently, several methods were presented to address the mixed FF and NF source localization problem. In [15], a two-stage multiple signal classification (TSMUSIC) method was proposed by constructing two special fourth-order cumulant (FOC) matrices and conducting two one-dimensional (1-D) spectral searches. Based on the TSMUSIC method, the oblique projection based MUSIC (OPMUISC) method employing the second-order statistics (SOS) was developed [16], with a much reduced computational complexity. By exploiting the eigenstructure differences between FF and NF covariance matrices, the spatial differencing based method was introduced in [17], which can provide an improved classification and localization accuracy. A few other source localization methods for mixed FF and NF sources were proposed in [18]-[22], which are also based on either FOC or SOS.

All the mixed source localization methods mentioned above are based on the point source model, assuming that the source signal propagates along a single straight path to the array. However, in practice, multipath transmission always exists and cannot be ignored in most cases. Therefore, a scattered or distributed source model is more appropriate [23]. In general, the distributed sources can be further categorized into coherently distributed (CD, i.e., the signal components arriving from different paths of the same source are coherent) and incoherently distributed (ID, i.e., the signal components arriving from different paths of the same source are not coherent) sources, which correspond to slowly time-varying channels and rapidly time-varying channels, respectively [24]. For a rapidly time-varying channel, the channel coherency time is supposed to be much smaller than the observation period, while for a slowly time-varying channel, the situation is just

Manuscript received March 16, 2022. This work was supported in part by the National Natural Science Foundation of China (NSFC) under Grants 62001256, 61871246 and 61971249, and in part by the Project of Scientific Research Ability Improvement of Young Teachers in Guangxi Province under Grant 2021KY0052. (*Corresponding Authors: Wei Liu and Hua Chen*).

Y. Tian, H. Chen and G. Wang are with the Faculty of Information Science and Engineering, Ningbo University, Ningbo 315211, China (e-mail: tianfield@126.com; dkchenhua0714@hotmail.com; wanggang@nbu.edu.cn).

X. Gao is with the School of Information Science and Engineering, Yanshan University, Qinhuangdao 066004, China. (e-mail: 13722513680@163.com).

W. Liu is with the Department of Electronic and Electrical Engineering, University of Sheffield, Sheffield S1 3JD, U.K. (e-mail: w.liu@sheffield.ac.uk).

Y. Qin is with the School of Electronic Engineering, Guangxi Normal University, Guilin, Guangxi 541004, China (e-mail: qinyunbai@gxnu.edu.cn).

the opposite. Many methods have been proposed for the localization of distributed sources; examples include the dimension reduction MUSIC algorithm for maximal noncircularity rated signals (DRNC-MUSIC) [25], the estimating signal parameters via rotational invariance technique (ESPRIT) [26] or unitary ESPRIT [27], and the perturbed sparse reconstruction based method [28] for CD sources, or the dispersed signal parameter estimator (DISPARE) [29] employing the asymptotic orthogonality property between the quasi-signal and noise subspaces, the ESPRIT [30], [31], the Beamspace [32], the covariance matching estimation techniques (COMET) [33] and the low-rank matrix recovery [34] based methods exploiting the low-rank property of the joint angular-frequency distribution matrix for ID sources. These methods are developed for pure FF distributed sources. Recently, Chaaya [35] and Yang [36] considered the NF CD and NF ID source localization problem, and exploited the MUSIC criterion and low-rank matrix recovery technique for DOA and range estimation, respectively. They further revealed that the closer the sources are to the array, the more scattered they seem to be. These two approaches are good attempts for localization of NF distributed sources. However, to our best knowledge, there are no reports for source localization under the coexistence of FF and NF distributed sources yet.

To fill this gap, a mixed FF and NF source localization method utilizing a two-stage RARE estimator is proposed in this paper, where the ID source model with generalized array manifold (GAM) is considered. Such a model can be obtained by applying the first-order approximation of Taylor expansion and has been proved in [37] that it is a good alternative to the accurate mathematical ID model employed in wireless channels with small local scattering. At the first stage, nominal DOA estimation of FF sources is performed by constructing a 1-D FF RARE spectral function employing the property of generalized shift invariance, which is formed by dividing the whole linear array into two subarrays, and it always holds for FF ID sources; at the second stage, the oblique projection operator is applied to eliminate the component of FF sources and simultaneously obtain nominal DOA and range (usually mean the assumed center DOA and range for a distributed source) information of NF ID sources using another two 1-D spectral functions, where the oblique projection operator provides a suitable way to integrate prior knowledge into subspace-based methods [38], and for our solution, it aims to cancel the influence of estimated FF parameters on subsequent estimation of the unknown NF parameters; finally, with the aid of estimated nominal DOA and range parameters, angular and range spreads (defined as the standard deviation of angular and range distributions around the nominal DOA and range) are estimated.

The main contributions of the paper can be summarized into the following three aspects:

- It is the first time to address the mixed FF and NF source localization problem considering the ID source model. By jointly exploiting the shift invariance of FF GAM, the oblique projection and the manifold separation technique (MST, a technique for separating an array manifold matrix into two parts, one of which contains information for only one parameter of interest, such as DOA), the proposed method can perform localization and source types classification effectively without multi-dimensional spectral search and parameters pairing.
- It is verified that the Akaike's information criterion (AIC) combined with the output of 1-D RARE spectral function can be used to achieve mixed FF and NF distributed source enumeration effectively, and its suitability in different signal-to-noise ratio (SNR), different number of antennas and snapshots is analyzed.
- An analysis of the proposed method in terms of required number of antennas, estimation accuracy and computational complexity is provided. Moreover, an approximate Cramér-Rao bound (CRB) for the considered scenario is derived, which provides a suitable reference for performance assessment of the proposed method.

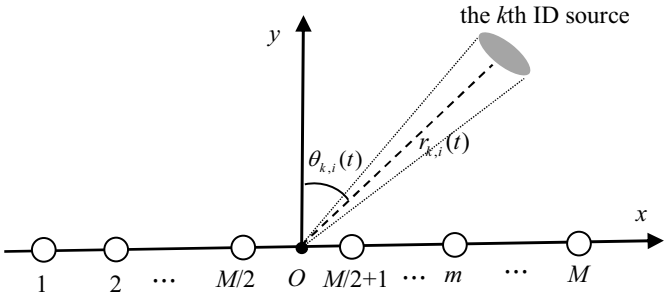

Fig. 1. The adopted uniform linear array structure.

The rest of this paper is organized as follows. In Section II, the system model with associated assumptions is given. In Section III, the proposed method is presented in detail. In Section IV, performance analysis about the proposed method is provided, followed by the approximate CRB for the mixed FF and NF ID sources. Numerical simulations are given in Section V, and conclusions are drawn in Section VI.

Notations: Lowercase (uppercase) boldface symbols represent vectors (matrices). The superscripts $(\cdot)^*$, $(\cdot)^T$, $(\cdot)^H$, $(\cdot)^{-1}$, $(\cdot)^\dagger$ and $(\cdot)^{1/2}$ denote the conjugate, transpose, conjugate transpose, inverse, pseudo-inverse and the square root operations, respectively. $\mathbb{E}[\cdot]$, $\mathrm{diag}\{\cdot\}$, $\det[\cdot]$ and $\mathrm{vec}(\cdot)$ stand for statistical expectation, diagonalization, determinant and vectorization, respectively. $\otimes$ represents the Kronecker product; and $\odot$ the Hadamard-Schur product. $\mathbf{I}_M$ is an $M \times M$ identity matrix, and $\delta(\cdot)$ the Kronecker delta function.

II. System Model

Consider K uncorrelated narrowband ID sources containing K_1 FF sources and $K - K_1$ NF sources impinging on an M-element uniform linear array (ULA), as depicted in Fig. 1, where M is even. The distance d between adjacent elements is a quarter to the wavelength λ and all the impinging signals are in the same frequency band. Due to scattering, the received

signal $\mathbf{y}(t) \in \mathbb{C}^{M\times 1}$ at the array is given by

$$\mathbf{y}(t) = \sum_{k=1}^{K_1} s_k(t) \sum_{i=1}^{N_k} \gamma_{k,i}(t)\mathbf{a}(\theta_{k,i}(t)) + \sum_{k=K_1+1}^{K} s_k(t)\cdot \sum_{i=1}^{N_k} \gamma_{k,i}(t)\mathbf{a}(\theta_{k,i}(t), r_{k,i}(t)) + \mathbf{n}(t), \quad (1)$$

where $s_k(t)$ and N_k are the complex-valued signal and the number of multipaths/scatters of the kth ID source, respectively. $\mathbf{n}(t) \in \mathbb{C}^{M\times 1}$ is the complex-valued additive noise. $\gamma_{k,i}(t)$, $\theta_{k,i}(t)$ and $r_{k,i}(t)$ are the complex-valued path gain, the real-valued DOA, and the real-valued range of the ith path from the kth source, respectively, which satisfy $-\pi/2 \le \theta_{k,i}(t) < \pi/2$ and $\lambda/2\pi < r_{k,i}(t) < 2D^2/\lambda$ (i.e., the NF source is located at the Fresnel region [4], [15]), where $D = (M-1)d$ is the array aperture. Taking the center of the array as the reference point, the array steering vectors $\mathbf{a}(\theta_{k,i}(t))$ of the FF ID source and $\mathbf{a}(\theta_{k,i}(t), r_{k,i}(t))$ of the NF ID source are given by

$$\mathbf{a}(\theta_{k,i}(t)) = [e^{j\frac{1-M}{2}w_{k,i}(t)}, \ldots, e^{j\frac{M-1}{2}w_{k,i}(t)}]^T, \quad (2)$$

$$\mathbf{a}(\theta_{k,i}(t), r_{k,i}(t)) = [e^{j\frac{1-M}{2}w_{k,i}(t)+j(\frac{1-M}{2})^2\phi_{k,i}(t)}, \ldots, e^{j\frac{M-1}{2}w_{k,i}(t)+j(\frac{M-1}{2})^2\phi_{k,i}(t)}]^T, \quad (3)$$

with

$$w_{k,i}(t) = -2\pi d\sin(\theta_{k,i}(t))/\lambda, \quad (4)$$

$$\phi_{k,i}(t) = \pi d^2\cos^2(\theta_{k,i}(t))/r_{k,i}(t)/\lambda. \quad (5)$$

According to the scattering model [33], the DOA and range can be expressed as

$$\theta_{k,i}(t) = \theta_k + \tilde{\theta}_{k,i}(t),\ r_{k,i}(t) = r_k + \tilde{r}_{k,i}(t), \quad (6)$$

where θ_k and r_k are the nominal DOA and nominal range for the kth source, and they are the mean values of $\theta_{k,i}(t)$ and $r_{k,i}(t)$, respectively. $\tilde{\theta}_{k,i}(t)$ and $\tilde{r}_{k,i}(t)$ are the corresponding random angular and range deviations with zero-mean and standard deviations σ_{θ_k} and σ_{r_k}, which are defined as angular and range spreads, respectively.

In this paper, we make the following assumptions:

- The path gains $\gamma_{k,i}(t)$ are temporally independent and identically distributed (i.i.d.) complex-valued zero-mean random variables with covariance
$$\mathbb{E}\{\gamma_{k,i}(t)\gamma^*_{\tilde{k},\tilde{i}}(\tilde{t})\} = \frac{\sigma^2_{\gamma_k}}{N_k}\delta(k-\tilde{k})\delta(i-\tilde{i})\delta(t-\tilde{t}). \quad (7)$$
- The angular deviations $\tilde{\theta}_{k,i}(t)$ and range deviations $\tilde{r}_{k,i}(t)$ are temporally i.i.d. real-valued Gaussian random variables, and their corresponding covariances are
$$\mathbb{E}\{\tilde{\theta}_{k,i}(t)\tilde{\theta}_{\tilde{k},\tilde{i}}(\tilde{t})\} = \sigma^2_{\theta_k}\delta(k-\tilde{k})\delta(i-\tilde{i})\delta(t-\tilde{t}), \quad (8)$$
$$\mathbb{E}\{\tilde{r}_{k,i}(t)\tilde{r}_{\tilde{k},\tilde{i}}(\tilde{t})\} = \sigma^2_{r_k}\delta(k-\tilde{k})\delta(i-\tilde{i})\delta(t-\tilde{t}). \quad (9)$$
- The incoming source signals are statistically independent, zero-mean complex random processes. The noise is zero-mean, complex circular Gaussian, and spatially uniformly white, with covariance matrix $\mathbb{E}[\mathbf{n}(t)\mathbf{n}^H(t)] = \sigma_n^2\mathbf{I}_M$.
- The source signals, angular deviations, range deviations and path gains are uncorrelated with each other.
- The angular spread σ_{θ_k} and range spread σ_{r_k} are rather small and the number of multipaths N_k of each signal is large.
- To avoid phase ambiguities, the number of ID sources should satisfy $K \le (M-1)/2$ and $K - K_1 \le M/6$.

Remark 1: As in [29]-[33], the DTs are located in a small angle scattering environment (i.e., the angular spreads $\{\sigma_{\theta_k}\}_{k=1}^K$ are rather small). Under the condition of general spherical scattering, it can be found that there is a relationship between the angular and range deviations, i.e., $\max\{\tilde{r}_{k,i}(t)\} = r_k \cdot \tan(\max\{\tilde{\theta}_{k,i}(t)\})$, which implies that the assumption on small angular and range spreads is reasonable.

Under small angular and range spreads, we obtain the general array steering vectors of $\mathbf{a}(\theta_{k,i}(t))$ and $\mathbf{a}(\theta_{k,i}(t), r_{k,i}(t))$ by exploiting the first-order Taylor expansion around the nominal DOA θ_k and nominal range r_k, which are written as

$$\mathbf{a}(\theta_{k,i}(t)) \approx \mathbf{a}(\theta_k) + \mathbf{d}(\theta_k)\cdot\tilde{\theta}_{k,i}(t), k = 1, \ldots, K_1, \quad (10)$$

$$\mathbf{a}(\theta_{k,i}(t), r_{k,i}(t)) \approx \mathbf{a}(\theta_k, r_k) + \mathbf{d}_\theta(\theta_k, r_k)\cdot\tilde{\theta}_{k,i}(t) + \mathbf{d}_r(\theta_k, r_k)\cdot\tilde{r}_{k,i}(t), k = K_1+1, \ldots, K, \quad (11)$$

respectively, where $\mathbf{d}(\theta_k) = \partial\mathbf{a}(\theta_k)/\partial\theta_k$, $\mathbf{d}_\theta(\theta_k, r_k) = \partial\mathbf{a}(\theta_k, r_k)/\partial\theta_k$ and $\mathbf{d}_r(\theta_k, r_k) = \partial\mathbf{a}(\theta_k, r_k)/\partial r_k$.

Subsequently, the received signal in (1) can be approximately expressed as

$$\mathbf{y}(t) \approx \sum_{k=1}^{K_1}(\mathbf{a}(\theta_k)v_{k0}(t) + \mathbf{d}(\theta_k)v_{k1}(t)) + \sum_{k=K_1+1}^{K}(\mathbf{a}(\theta_k, r_k)v_{k0}(t) + \mathbf{d}_\theta(\theta_k, r_k)v_{k1}(t) + \mathbf{d}_r(\theta_k, r_k)v_{k2}(t)) + \mathbf{n}(t), \quad (12)$$

where

$$v_{k0}(t) = s_k(t)\sum_{i=1}^{N_k}\gamma_{k,i}(t), \quad (13)$$

$$v_{k1}(t) = s_k(t)\sum_{i=1}^{N_k}\gamma_{k,i}(t)\tilde{\theta}_{k,i}(t), \quad (14)$$

$$v_{k2}(t) = s_k(t)\sum_{i=1}^{N_k}\gamma_{k,i}(t)\tilde{r}_{k,i}(t). \quad (15)$$

As a result, the received signal with GAM in case of mixed FF and NF ID sources is written as

$$\mathbf{y}(t) \approx \mathbf{A}_F(\theta)\mathbf{V}_F(t) + \mathbf{A}_N(\theta, r)\mathbf{V}_N(t) + \mathbf{n}(t) = \bar{\mathbf{A}}\bar{\mathbf{V}}(t) + \mathbf{n}(t), \quad (16)$$

where $\bar{\mathbf{A}} = [\mathbf{A}_F(\theta), \mathbf{A}_N(\theta, r)]$ is defined as the GAM, $\bar{\mathbf{V}}(t) = [\mathbf{V}_F(t), \mathbf{V}_N(t)]^T$, and

$$\mathbf{A}_F(\theta) = [\mathbf{a}(\theta_1), \mathbf{d}(\theta_1), \ldots, \mathbf{a}(\theta_{K_1}), \mathbf{d}(\theta_{K_1})], \quad (17)$$

$$\mathbf{A}_N(\theta,r)=[\mathbf{a}(\theta_{K_1+1},r_{K_1+1}),\mathbf{d}_\theta(\theta_{K_1+1},r_{K_1+1}),\mathbf{d}_r(\theta_{K_1+1},r_{K_1+1}),\ldots,\mathbf{a}(\theta_K,r_K),\mathbf{d}_\theta(\theta_K,r_K),\mathbf{d}_r(\theta_K,r_K)], \quad (18)$$

$$\mathbf{V}_F(t)=[v_{10}(t),v_{11}(t),\ldots,v_{K_10}(t),v_{K_11}(t)]^T, \quad (19)$$

$$\mathbf{V}_N(t)=[v_{(K_1+1)0}(t),v_{(K_1+1)1}(t),v_{(K_1+1)2}(t),\ldots,v_{K0}(t),v_{K1}(t),v_{K2}(t)]^T. \quad (20)$$

According to (16) and the properties of $\tilde{\theta}_{k,i}(t)$, $\tilde{r}_{k,i}(t)$, $\gamma_{k,i}(t)$ and $s_k(t)$, the array covariance matrix can be expressed as

$$\begin{aligned}\mathbf{R}&=\mathbb{E}\left\{\mathbf{y}(t)\mathbf{y}^H(t)\right\}=\bar{\mathbf{A}}\mathbf{\Lambda}\bar{\mathbf{A}}^H+\sigma_n^2\mathbf{I}_M\\&=\mathbf{A}_F(\theta)\mathbf{\Lambda}_F\mathbf{A}_F^H(\theta)+\mathbf{A}_N(\theta,r)\mathbf{\Lambda}_N\mathbf{A}_N^H(\theta,r)+\sigma_n^2\mathbf{I}_M,\end{aligned} \quad (21)$$

where $\mathbf{\Lambda}=\mathbb{E}(\bar{\mathbf{V}}^H\bar{\mathbf{V}})=\mathrm{diag}\left\{\mathbf{\Lambda}_F,\mathbf{\Lambda}_N\right\}$ with

$$\mathbf{\Lambda}_F=\mathrm{diag}\{\rho_1,\rho_1\sigma_{\theta_1}^2,\ldots,\rho_{K_1},\rho_{K_1}\sigma_{\theta_{K_1}}^2\}, \quad (22)$$

$$\mathbf{\Lambda}_N=\mathrm{diag}\{\rho_{K_1+1},\rho_{K_1+1}\sigma_{\theta_{K_1+1}}^2,\rho_{K_1+1}\sigma_{r_{K_1+1}}^2,\ldots,\rho_K,\rho_K\sigma_{\theta_K}^2,\rho_K\sigma_{r_K}^2\}, \quad (23)$$

$\rho_k=P_k\sigma_{\gamma_k}^2$ and P_k is the power of the kth source signal.

III. The Proposed Method

A. Source Enumeration of Virtual Sources

The proposed solution belongs to the subspace framework. Therefore, both the number of FF and that of NF ID sources are required to be estimated, since they are essential for distinguishing signal and noise subspaces. It is observed from (16)-(20) that $\mathbf{y}(t)$ can be regarded as containing $3K-K_1$ sources under the ID source model, which is different from that of point and CD source model. Since the number of these sources is larger than that of actual sources K, we name them as virtual sources here. So far, there are no reports for source enumeration of ID sources. Fortunately, through our analysis and extensive numerical simulations, it is found that AIC can be exploited for this task under certain conditions. The objective function of AIC is given by

$$\hat{\bar{K}}=\arg\min_{\bar{K}}2L(M-\bar{K})\log\left(\frac{\frac{1}{M-\bar{K}}\sum_{i=\bar{K}+1}^{M}\hat{\lambda}_i}{\prod_{i=\bar{K}+1}^{M}\hat{\lambda}_i^{\frac{1}{M-\bar{K}}}}\right)+v_{\bar{K}}, \quad (24)$$

where $v_{\bar{K}}=2[\bar{K}(2M-\bar{K})+1]$, $\bar{K}$ is the assumed number of virtual sources, and its corresponding covariance matrix is denoted as $\mathbf{R}^{(\bar{K})}$, whose eigenvalues $\hat{\lambda}_1,\ldots,\hat{\lambda}_M$ are in descending order. The following proposition shows the suitability of the AIC for source enumeration of the considered scenario.

Proposition 1: For the virtual source enumeration of mixed FF and NF ID sources, the AIC is effective, provided that the following inequality holds

$$10^{\mathrm{SNR}/10}\cdot\sigma_{\gamma,\alpha}^2\cdot\sigma_{\theta,r}^2>\frac{1}{\sqrt{ML}}, \quad (25)$$

where $\mathrm{SNR}=10\log_{10}(P_k/\sigma_n^2)$, $\sigma_{\gamma,\alpha}^2$ and $\sigma_{\theta,r}^2$ represent the minimum value of $\{\sigma_{\gamma_k}^2\alpha_k|k=1,\ldots,K\}$ and $\{\sigma_{\theta_k}^2,\sigma_{r_k}^2|k=1,\ldots,K\}$, respectively, and α_k the eigenvalues of $\frac{1}{M}\bar{\mathbf{A}}\bar{\mathbf{A}}^H$.

Proof: See Appendix A. □

Remark 2: It can be seen from Proposition 1 that the virtual source enumeration performance is proportional to SNR, M, L, $\sigma_{\gamma,\alpha}^2$ and $\sigma_{\theta,r}^2$. Since small angular and range spreads are assumed, (24) will yield accurate source enumeration result, and $\hat{\bar{K}}=3K-K_1$, in case of relatively large SNR, M and L (also see the simulation result for further verification).

B. Nominal DOA Estimation of FF Sources

Based on the result of virtual source enumeration and the principle of shift invariance of GAM of FF ID sources, nominal DOA estimation of FF ID sources is derived. Specifically, we divide the array into two subarrays with the same number of sensors, subarray1 contains the first $M-1$ sensors, while subarray2 contains the last $M-1$ sensors. Let $\bar{\mathbf{A}}_1$ and $\bar{\mathbf{A}}_2$ denote the GAMs of subarray1 and subarray2, respectively, $\bar{\mathbf{A}}_n=[\bar{\mathbf{A}}_n(\theta),\bar{\mathbf{A}}_n(\theta,r)]$, $\bar{\mathbf{A}}_n(\theta_k)=[\bar{\mathbf{a}}_n(\theta_k),\bar{\mathbf{d}}_n(\theta_k)]$, $\bar{\mathbf{A}}_n(\theta_k,r_k)=[\bar{\mathbf{a}}_n(\theta_k,r_k),\bar{\mathbf{d}}_{\theta n}(\theta_k,r_k),\bar{\mathbf{d}}_{rn}(\theta_k,r_k)]$, $n=1,2$. $\{\bar{\mathbf{a}}_1(\theta_k),\bar{\mathbf{d}}_1(\theta_k)\}$ and $\{\bar{\mathbf{a}}_2(\theta_k),\bar{\mathbf{d}}_2(\theta_k)\}$ represent the general steering vectors of FF ID sources related to subarray1 and subarray2, respectively. Then, the following shift invariance property holds

$$\bar{\mathbf{a}}_2(\theta_k)=\mathbf{\Phi}_{k1}\bar{\mathbf{a}}_1(\theta_k),\ \bar{\mathbf{d}}_2(\theta_k)=\mathbf{\Phi}_{k2}\bar{\mathbf{d}}_1(\theta_k), \quad (26)$$

where

$$\mathbf{\Phi}_{k1}=\mathrm{diag}\{e^{j\omega_k},\ldots,e^{j\omega_k}\}, \quad (27)$$

$$\mathbf{\Phi}_{k2}=\mathrm{diag}\{\frac{3-M}{1-M}e^{j\omega_k},\ldots,\frac{M-1}{M-3}e^{j\omega_k}\}, \quad (28)$$

with $\omega_k=-2\pi d\sin(\theta_k)/\lambda$, $\mathbf{\Phi}_{k1},\mathbf{\Phi}_{k2}\in\mathbb{C}^{(M-1)\times(M-1)}$.

Performing eigenvalue decomposition (EVD) yields

$$\mathbf{R}=\mathbf{U}_s\mathbf{\Sigma}_s\mathbf{U}_s^H+\mathbf{U}_n\mathbf{\Sigma}_n\mathbf{U}_n^H, \quad (29)$$

where $\mathbf{\Sigma}_s$ and $\mathbf{\Sigma}_n$ are diagonal matrices comprising the largest $3K-K_1$ and remaining smallest eigenvalues of $\mathbf{R}$, respectively. $\mathbf{U}_s$ and $\mathbf{U}_n$ are $M\times(3K-K_1)$-dimensional signal subspace and $M\times(M-3K+K_1)$-dimensional noise subspace, respectively. Then, $\mathbf{U}_s$ can be partitioned as

$$\mathbf{U}_s=\begin{bmatrix}\mathbf{U}_{s1}\\ the\ last\ row\end{bmatrix}=\begin{bmatrix}the\ first\ row\\ \mathbf{U}_{s2}\end{bmatrix}, \quad (30)$$

which satisfies $\mathbf{U}_s=\bar{\mathbf{A}}\mathbf{T}$, $\mathbf{U}_{s1}=\bar{\mathbf{A}}_1\mathbf{T}$ and $\mathbf{U}_{s2}=\bar{\mathbf{A}}_2\mathbf{T}$, where $\mathbf{T}$ is an invertible $(3K-K_1)\times(3K-K_1)$-dimensional matrix.

Define $\mathbf{D}(\theta)$ as

$$\begin{aligned}\mathbf{D}(\theta)&=\mathbf{U}_{s2}-\mathbf{\Psi}(\theta)\mathbf{U}_{s1}\\&=(\bar{\mathbf{A}}_2-\mathbf{\Psi}(\theta)\bar{\mathbf{A}}_1)\mathbf{T}=\mathbf{Q}(\theta)\mathbf{T}.\end{aligned} \quad (31)$$

where

$$\mathbf{\Psi}(\theta)=\mathrm{diag}\{e^{j\omega},\ldots,e^{j\omega}\}\in\mathbb{C}^{(M-1)\times(M-1)}, \quad (32)$$

$$\mathbf{Q}(\theta)=[\mathbf{q}_{f_1}(\theta),\mathbf{q}_{df_1}(\theta),\ldots,\mathbf{q}_{n_K}(\theta,r),\mathbf{q}_{dn_K}(\theta,r),\mathbf{q}_{dr_K}(\theta,r)], \quad (33)$$

$$\mathbf{q}_{f_k}(\theta) = (\mathbf{\Phi}_{k1} - \mathbf{\Psi}(\theta))\bar{\mathbf{a}}_1(\theta_k),\ k = 1, \ldots, K_1, \tag{34}$$

$$\mathbf{q}_{df_k}(\theta) = (\mathbf{\Phi}_{k2} - \mathbf{\Psi}(\theta))\bar{\mathbf{d}}_1(\theta_k),\ k = 1, \ldots, K_1, \tag{35}$$

$$\mathbf{q}_{n_k}(\theta, r) = \bar{\mathbf{a}}_2(\theta_k, r_k) - \mathbf{\Psi}(\theta)\bar{\mathbf{a}}_1(\theta_k, r_k), \quad k = K_1 + 1, \ldots, K, \tag{36}$$

$$\mathbf{q}_{dn_k}(\theta, r) = \bar{\mathbf{d}}_{\theta 2}(\theta_k, r_k) - \mathbf{\Psi}(\theta)\bar{\mathbf{d}}_{\theta 1}(\theta_k, r_k), \quad k = K_1 + 1, \ldots, K, \tag{37}$$

$$\mathbf{q}_{dr_k}(\theta, r) = \bar{\mathbf{d}}_{r2}(\theta_k, r_k) - \mathbf{\Psi}(\theta)\bar{\mathbf{d}}_{r1}(\theta_k, r_k), \quad k = K_1 + 1, \ldots, K. \tag{38}$$

It can be found that $\mathbf{q}_{f_k}(\theta)$ will become zeros when $\theta = \theta_k$ $k = 1, \ldots, K_1$, which implies that if an ID source is FF, $\mathbf{D}(\theta)$ is rank deficient and the determinant of $\mathbf{D}^H(\theta)\mathbf{D}(\theta)$ is zero. Consequently, we can obtain the nominal DOA estimation of FF ID sources from the following 1-D RARE spectral function

$$\eta_F(\hat{\theta}) = \{\det[\mathbf{D}^H(\theta)\mathbf{D}(\theta)]\}^{-1}. \tag{39}$$

According to the subspace theory and the numerical simulation results, (39) will produce K_1 sources, which corresponds to the FF ID sources. With K_1 and $\hat{\hat{K}}$, the number of NF ID sources is calculated by $K_2 = \frac{\hat{\hat{K}} - 2K_1}{3}$.

Remark 3: In some practical systems, such as cellular communication systems, prior knowledge about the total number of DTs K could be obtained through DTs registration to base station (BS), and thus K_1, K_2 can be obtained easily via $K_1 = 3K - \hat{\hat{K}}$ and $K_2 = \hat{\hat{K}} - 2K$. In addition, in a special case of $\hat{\hat{K}}$, such as $\hat{\hat{K}} = 2, 3, 5, 7$, we can obtain the number of FF and NF sources without other auxiliary information. For example, if $\hat{\hat{K}} = 5$, then both K_1 and K_2 can only be equal to 1; if $\hat{\hat{K}} = 7$, then K_1 and K_2 can only be equal to 2 and 1, respectively.

C. Nominal DOA and Range Estimation of NF ID Sources

The oblique projection (OP) technique is an efficient way to distinguish mixed FF and NF sources. Let $\mathbf{E}_{\mathbf{A}_F\mathbf{A}_N}$ be an oblique projection matrix, which is idempotent and has the following property [16]:

$$\mathbf{E}_{\mathbf{A}_F\mathbf{A}_N}\mathbf{A}_F(\theta) = \mathbf{0}, \mathbf{E}_{\mathbf{A}_F\mathbf{A}_N}\mathbf{A}_N(\theta, r) = \mathbf{A}_N(\theta, r). \tag{40}$$

By applying such a matrix on $\mathbf{y}(t)$, we then have

$$\begin{aligned}\mathbf{z}(t) &= (\mathbf{I}_M - \mathbf{E}_{\mathbf{A}_F\mathbf{A}_N})\mathbf{y}(t) \\ &= \mathbf{A}_N(\theta, r)\mathbf{V}_N(t) + (\mathbf{I}_M - \mathbf{E}_{\mathbf{A}_F\mathbf{A}_N})\mathbf{n}(t).\end{aligned} \tag{41}$$

It can be seen that $\mathbf{z}(t)$ only contains the information of NF ID sources, which provides a direct and effective path for subsequent realization of NF ID source localization. With the estimated nominal DOAs of FF ID sources, the GAM of FF ID sources can be reconstructed as

$$\mathbf{A}_F(\hat{\theta}) = [\mathbf{a}(\hat{\theta}_1), \mathbf{d}(\hat{\theta}_1), \ldots, \mathbf{a}(\hat{\theta}_{K_1}), \mathbf{d}(\hat{\theta}_{K_1})]. \tag{42}$$

Subsequently, $\mathbf{E}_{\mathbf{A}_F\mathbf{A}_N}$ is estimated by [38]

$$\mathbf{E}_{\mathbf{A}_F\mathbf{A}_N} = \mathbf{A}_F(\hat{\theta})(\mathbf{A}_F^H(\hat{\theta})\mathbf{R}^\dagger\mathbf{A}_F(\hat{\theta}))^{-1}\mathbf{A}_F^H(\hat{\theta})\mathbf{R}^\dagger. \tag{43}$$

Define $\mathbf{R}_z = \mathbb{E}\{\mathbf{z}(t)\mathbf{z}^H(t)\}$ as the covariance matrix of $\mathbf{z}(t)$, whose EVD is expressed as

$$\mathbf{R}_z = \mathbf{E}_s\mathbf{\Delta}_s\mathbf{E}_s^H + \mathbf{E}_n\mathbf{\Delta}_n\mathbf{E}_n^H, \tag{44}$$

where $\mathbf{E}_s$ and $\mathbf{E}_n$ are $M \times 3(K - K_1)$-dimensional signal subspace and $M \times (M - 3K + 3K_1)$-dimensional noise subspace, which correspond to $3(K - K_1)$ largest eigenvalues and the remaining small eigenvalues, respectively.

To achieve localization of NF ID sources efficiently, we rewrite the array steering vector $\mathbf{a}(\theta_k, r_k)$ as

$$\mathbf{a}(\theta_k, r_k) = \mathbf{B}(\theta_k)\mathbf{g}(\theta_k, r_k), \tag{45}$$

where $\mathbf{g}(\theta_k, r_k) = [e^{j(\frac{M-1}{2})^2\phi_k}, \ldots, e^{j(\frac{1}{2})^2\phi_k}]^T$, and

$$\mathbf{B}(\theta_k) = \begin{bmatrix} e^{j\frac{1-M}{2}\omega_k} & \cdots & 0 \\ \vdots & \ddots & \vdots \\ 0 & \cdots & e^{-j\frac{1}{2}\omega_k} \\ 0 & \cdots & e^{j\frac{1}{2}\omega_k} \\ \vdots & \iddots & \vdots \\ e^{j\frac{M-1}{2}\omega_k} & \cdots & 0 \end{bmatrix}. \tag{46}$$

Subsequently, it can be derived that

$$\mathbf{d}_\theta(\theta_k, r_k) = \mathbf{h}(\theta_k, r_k) \odot \mathbf{B}(\theta_k)\mathbf{g}(\theta_k, r_k), \tag{47}$$

$$\mathbf{d}_r(\theta_k, r_k) = \mathbf{f}(\theta_k, r_k) \odot \mathbf{B}(\theta_k)\mathbf{g}(\theta_k, r_k), \tag{48}$$

where

$$\begin{aligned}\mathbf{h}(\theta_k, r_k) = [&j\frac{1-M}{2}\varpi_k - j(\frac{1-M}{2})^2\psi_k, \ldots, \\ &j\frac{M-1}{2}\varpi_k - j(\frac{M-1}{2})^2\psi_k]^T,\end{aligned} \tag{49}$$

$$\mathbf{f}(\theta_k, r_k) = [-j(\frac{1-M}{2})^2\phi_k/r_k, \ldots, -j(\frac{M-1}{2})^2\phi_k/r_k]^T, \tag{50}$$

with $\varpi_k = -2\pi d\cos\theta_k/\lambda, \psi_k = \pi d^2\sin 2\theta_k/r_k/\lambda$.

According to the subspace theory, the following orthogonality properties hold

$$\begin{aligned}&\mathbf{a}^H(\theta_k, r_k)\mathbf{E}_n\mathbf{E}_n^H\mathbf{a}(\theta_k, r_k) \\ &\quad = \mathbf{g}^H(\theta_k, r_k)\mathbf{P}(\theta_k)\mathbf{g}(\theta_k, r_k) = 0,\end{aligned} \tag{51}$$

$$\begin{aligned}&\mathbf{a}^H(\theta_k, r_k)\mathbf{E}_n\mathbf{E}_n^H\mathbf{d}_\theta(\theta_k, r_k) \\ &\quad = \mathbf{g}^H(\theta_k, r_k)\mathbf{P}(\theta_k)\mathbf{g}(\theta_k, r_k) \odot \mathbf{h}(\theta_k, r_k) = 0,\end{aligned} \tag{52}$$

$$\begin{aligned}&\mathbf{a}^H(\theta_k, r_k)\mathbf{E}_n\mathbf{E}_n^H\mathbf{d}_r(\theta_k, r_k) \\ &\quad = \mathbf{g}^H(\theta_k, r_k)\mathbf{P}(\theta_k)\mathbf{g}(\theta_k, r_k) \odot \mathbf{f}(\theta_k, r_k) = 0,\end{aligned} \tag{53}$$

$$\begin{aligned}&\mathbf{d}_\theta^H(\theta_k, r_k)\mathbf{E}_n\mathbf{E}_n^H\mathbf{d}_\theta(\theta_k, r_k) = \mathbf{h}^H(\theta_k, r_k) \odot \\ &\quad \mathbf{g}^H(\theta_k, r_k)\mathbf{P}(\theta_k)\mathbf{g}(\theta_k, r_k) \odot \mathbf{h}(\theta_k, r_k) = 0,\end{aligned} \tag{54}$$

$$\begin{aligned}&\mathbf{d}_\theta^H(\theta_k, r_k)\mathbf{E}_n\mathbf{E}_n^H\mathbf{d}_r(\theta_k, r_k) = \mathbf{h}^H(\theta_k, r_k) \odot \\ &\quad \mathbf{g}^H(\theta_k, r_k)\mathbf{P}(\theta_k)\mathbf{g}(\theta_k, r_k) \odot \mathbf{f}(\theta_k, r_k) = 0,\end{aligned} \tag{55}$$

Algorithm 1: Localization for Mixed FF and NF ID Sources

1: Calculate the sampled covariance matrix $\hat{\mathbf{R}}$ and achieve source enumeration of virtual sources via (24).
2: Perform EVD on $\hat{\mathbf{R}}$ to obtain the signal subspace $\hat{\mathbf{U}}_s$, and then divide it into $\hat{\mathbf{U}}_{s1}$ and $\hat{\mathbf{U}}_{s2}$.
3: Construct $\mathbf{D}(\theta)$ according to (31), and further estimate nominal DOA and the number of FF ID sources from (39).
4: Reconstruct $\mathbf{A}_F(\hat{\theta})$ and calculate OP matrix $\mathbf{E}_{\mathbf{A}_F\mathbf{A}_N}$.
5: Form $\mathbf{z}(t)$ and $\hat{\mathbf{R}}_z$ utilizing $\mathbf{E}_{\mathbf{A}_F\mathbf{A}_N}$ and $\mathbf{y}(t)$.
6: Perform EVD on $\hat{\mathbf{R}}_z$ to find the noise subspace matrix $\hat{\mathbf{E}}_n$.
7: Conduct two 1-D spectral searches as shown in (57) and (58) to obtain nominal DOA and nominal range estimation of NF ID sources, respectively.
8: Reconstruct $\hat{\mathbf{\Lambda}}$ based on (59), and then determine $\hat{\sigma}_{\theta_k}$ and $\hat{\sigma}_{r_k}$ through (60)-(62).

$$\mathbf{d}_r^H(\theta_k,r_k)\mathbf{E}_n\mathbf{E}_n^H\mathbf{d}_r(\theta_k,r_k)=\mathbf{f}^H(\theta_k,r_k)\odot \mathbf{g}^H(\theta_k,r_k)\mathbf{P}(\theta_k)\mathbf{g}(\theta_k,r_k)\odot\mathbf{f}(\theta_k,r_k)=0, \quad (56)$$

where $\mathbf{P}(\theta_k)=\mathbf{B}^H(\theta_k)\mathbf{E}_n\mathbf{E}_n^H\mathbf{B}(\theta_k)$.

Eqs. (51)-(56) indicate that $\mathbf{P}(\theta_k)$ is singular if and only if $\theta=\theta_k$, $k=K_1+1,\ldots,K$. Therefore, the nominal DOA $\{\bar{\theta}_{K1+1},\ldots,\bar{\theta}_K\}$ of NF ID sources can be found by finding $K-K_1$ peaks of the following RARE spectral function

$$\eta_N(\bar{\theta})=\{\det[\mathbf{P}(\theta)]\}^{-1}. \quad (57)$$

With the estimated nominal DOAs of NF ID sources, the corresponding range estimation $[\bar{r}]_{K_1+1}^K$ can be obtained by

$$\bar{r}_k=\min_r\left[\mathbf{a}^H(\bar{\theta},r)\mathbf{E}_n\mathbf{E}_n^H\mathbf{a}(\bar{\theta},r)\right]^{-1}. \quad (58)$$

Remark 4: With application of the oblique projection technique, the proposed method is suitable for the special case where some of NF ID sources have the same nominal DOA as the FF ID sources.

D. Angular and Range Spreads Estimation

Since all nominal DOA and nominal range parameters have been estimated, $\mathbf{\Lambda}$ can be calculated by

$$\hat{\mathbf{\Lambda}}=\hat{\bar{\mathbf{A}}}^{\dagger}(\hat{\mathbf{R}}-\hat{\sigma}_n^2\mathbf{I}_M)(\hat{\bar{\mathbf{A}}}^{H})^{\dagger}, \quad (59)$$

where $\hat{\bar{\mathbf{A}}}=[\mathbf{A}_F(\hat{\theta}),\mathbf{A}_N(\bar{\theta},\bar{r})]$ is the estimation of GAM. $\hat{\sigma}_n^2$ is obtained by the average of the $(M-3K+K_1)$ smallest eigenvalues of $\hat{\mathbf{R}}$. According to the relationship of $\mathbf{\Lambda}$, the angular spread and range spread can be estimated via

$$\hat{\sigma}_{\theta_k}=\sqrt{\frac{[\hat{\mathbf{\Lambda}}]_{2k,2k}}{[\hat{\mathbf{\Lambda}}]_{2k-1,2k-1}}}, \quad k=1,2,\ldots,K_1, \quad (60)$$

$$\hat{\sigma}_{\theta_k}=\sqrt{\frac{[\hat{\mathbf{\Lambda}}]_{3k-K_1-1,3k-K_1-1}}{[\hat{\mathbf{\Lambda}}]_{3k-K_1-2,3k-K_1-2}}}, \quad k=K_1+1,\ldots,K, \quad (61)$$

$$\hat{\sigma}_{r_k}=\sqrt{\frac{[\hat{\mathbf{\Lambda}}]_{3k-K_1,3k-K_1}}{[\hat{\mathbf{\Lambda}}]_{3k-K_1-2,3k-K_1-2}}}, \quad k=K_1+1,\ldots,K. \quad (62)$$

The main steps of the proposed method are given in Algorithm 1, where $\hat{\chi}$ is the estimation result of χ with L snapshots, for example, $\mathbf{R}$ is estimated by $\hat{\mathbf{R}}=\sum_{t=1}^L\mathbf{y}(t)\mathbf{y}^H(t)/L$.

IV. Performance Analysis and Cramér-Rao Bound

A. Performance Analysis

In this subsection, the performance of the proposed method is discussed and analyzed from the following three aspects, i.e., number of required antennas, estimation accuracy in different scenarios and computational complexity.

1) Number of Required Antennas: The nominal DOA of both FF and NF ID sources are estimated based on the RARE principle. For the FF ID estimator, it can be obtained that $\mathrm{rank}(\mathbf{D}^H(\theta)\mathbf{D}(\theta))=\min\{3K-K_1,M-1\}$. Therefore, the sufficient conditions for the FF ID estimator are $3K-K_1\le M-1$ and $K_1\le K$, which directly yields $K_1\le K\le(M-1)/2$, while for the NF ID estimator, the maximum rank of $\mathbf{P}(\theta)$ is $\min\{M/2,M-3K_2\}$, where $K_2=K-K_1$. If $M/2>M-3K_2$, then $\mathbf{P}(\theta)$ is naturally rank-deficient, and the NF estimator fails. Hence, we have $M/2\le M-3K_2$ or equivalently, $K_2\le M/6$. That is, the proposed method can localize $K_2\le M/6$ NF ID sources and $M/2-K_2-1$ FF ID sources simultaneously using a ULA of M antennas, where K_2 is equal to the largest integer that satisfies the inequality condition, and M is even.

2) Estimation Accuracy: Compared with the point source model, the ID source model is rather complex, and there are more parameters that can affect the estimation accuracy of the related methods, including signal-to-noise ratio (SNR)/signal-to-interference-plus-noise ratio (SINR), the number of snapshots L, the number of antennas M, the angular spread σ_{θ_k} and the range spread σ_{r_k}. In general, the estimation accuracy increases as SINR, M and L increase. For the proposed method, the nominal DOA estimator of FF ID sources as shown in (39) can be considered as an implementation of a 1-D RARE estimator in the presence of σ_{θ_k} and NF ID interferences, and therefore, its corresponding SINR may not be very large even if SNR is large, which implies that it is difficult for the FF estimator to get close to the related Cramér-Rao bound (CRB). In fact, such a scenario has arised in various localization methods of ID sources (see [30]-[32] for details). In addition, it is obvious that the SINR decreases as σ_{θ_k} and σ_{r_k} increase, and hence the estimator's performance could degrade substantially with the increase of σ_{θ_k} and σ_{r_k}. The nominal DOA and nominal range estimators of NF ID sources formulated by (57) and (58) can be considered as another two 1-D estimators in the presence of residual item of FF ID sources; as a result, it is difficult to reach their corresponding CRBs due to influence of the FF ID estimator. Nevertheless, since we have assumed that σ_{θ_k} and σ_{r_k} are rather small, the proposed method can provide a good source classification and localization result, which will be verified by numerical simulations later.

3) Computational Complexity: Regarding the computational complexity, we consider the major part, including covariance matrix construction, EVD and 1-D spectral search. The proposed method constructs two $M\times M$-dimensional covariance matrices and implements their EVDs. In addition, the proposed method requires 1-D spectral search three times. Therefore, the resulting multiplications required by the proposed method are roughly in the order of $O(2M^2L+$

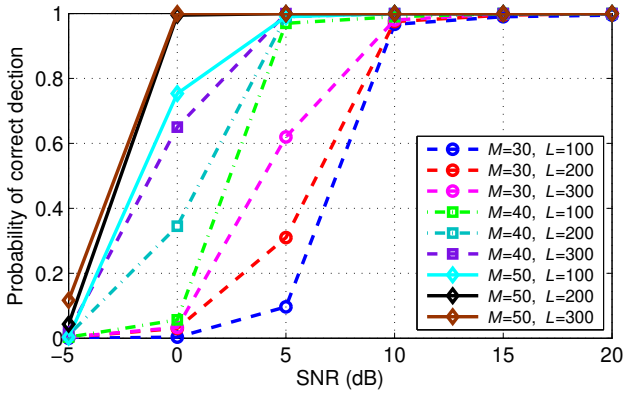

Fig. 2. Probabilities of correct detection/enumeration versus SNR, M and L for one FF and one NF ID sources with $\{\theta_1 = 10°, \sigma_{\theta_1} = 2°\}$, $\{\theta_2 = 30°, \sigma_{\theta_2} = 1°, r_2 = 2\lambda, \sigma_{r_2} = r_2 \cdot \tan(\sigma_{\theta_2})\}$.

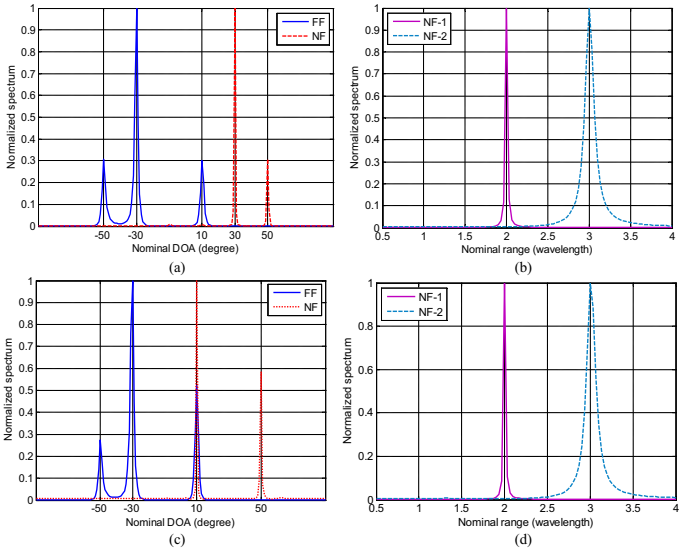

Fig. 3. Spatial spectrums of the proposed method for three FF ID sources and two NF ID sources, SNR=10 dB, $M = 40$, $L = 200$: (a) and (b) for scenario 1; (c) and (d) for scenario 2.

$\frac{3}{2}M^3 + M^2G_1 + M^2G_2)$, which is similar with that of the OPMUSIC method for point source model [16], where G_1 and G_2 are the search sizes for estimating nominal DOA and range, respectively.

B. Approximate Cramér-Rao Bound

In order to assess the performance of the proposed method, the Cramér-Rao bound for the considered mixed ID sources is derived. Define the unknown parameters vector as $\boldsymbol{\xi} = [\boldsymbol{\mu}^T, \boldsymbol{\nu}^T]^T$, where $\boldsymbol{\mu} = [\boldsymbol{\theta}^T, \mathbf{r}^T, \boldsymbol{\sigma}_\theta{}^T, \boldsymbol{\sigma}_r{}^T]^T = [\theta_1, \ldots, \theta_K, r_{K_1+1}, \ldots, r_K, \sigma_{\theta_1}, \ldots, \sigma_{\theta_K}, \sigma_{r_{K_1+1}}, \ldots, \sigma_{r_K}]^T$ are the parameters of interest, and $\boldsymbol{\nu} = [\rho_1, \ldots, \rho_K, \sigma_n^2]^T$ are the remaining parameters.

Define

$$(\mathbf{R}^{-T/2} \otimes \mathbf{R}^{-1/2}) \left[\frac{\partial \mathbf{r}}{\partial \boldsymbol{\mu}^T} \quad \frac{\partial \mathbf{r}}{\partial \boldsymbol{\nu}^T} \right] \overset{def}{=} [\mathbf{W} \quad \mathbf{V}], \tag{63}$$

and then, the approximate CRB concerning the parameters of interest is given by

$$\mathrm{CRB}(\boldsymbol{\mu}) = \frac{1}{L} \left[\mathbf{W}^H \boldsymbol{\Pi}_V^{\perp} \mathbf{W} \right]^{-1}, \tag{64}$$

where $\boldsymbol{\Pi}_V^{\perp} = \mathbf{I} - \mathbf{V}(\mathbf{V}^H\mathbf{V})^{-1}\mathbf{V}^H$. Detailed derivation of (64) is provided in Appendix B.

V. Simulations and Results

In this section, the performance of the proposed method is evaluated and compared with the TSMUSIC method [15] and the OPMUSIC method [16]. Additionally, the approximate CRB of the proposed estimator is also calculated for performance assessment. Note that the required number of antennas M of the proposed method is even, whereas that $\bar{M}$ of the TSMUSIC method and the OPMUSIC method is odd, hence we set $\bar{M} = M + 1$ for comparison in the simulations. All the impinging signals are of equal power and BPSK modulated, and the average received SNR from the kth DT is defined as $10\log_{10}(P_K/\sigma_n^2)$. For the adopted M-element ULA, the Fresnel region is $0.159\lambda < r < 0.125(M-1)^2\lambda$. The path gain variances are fixed at $\sigma_{r_k}^2 = 1$ and the number of multipaths is $N_k = 50$ except for the seventh simulation, $k = 1, \ldots, K$. The results are measured by the root mean square error (RMSE) from the average results of 500 independent Monte-Carlo trials, defined as

$$\mathrm{RMSE} = \sqrt{\frac{1}{500K} \sum_{k=1}^{K} \sum_{c=1}^{500} (\hat{\beta}_{k,c} - \beta_k)^2}, \tag{65}$$

where $\hat{\beta}_{k,c}$ is the estimate of β_k in the cth trial.

In the first simulation, we examine empirical probabilities of correct detection of the number of ID sources with different SNRs, M and L. One FF and one NF ID sources with their parameters $\{\theta_1 = 10°, \sigma_{\theta_1} = 2°\}$, $\{\theta_2 = 30°, \sigma_{\theta_2} = 1°, r_2 = 2\lambda, \sigma_{r_2} = r_2 \cdot \tan(\sigma_{\theta_2})\}$ are considered. It can be seen from Fig. 2 that the performance of source enumeration improves as SNR, M and L increase, which is consistent with Proposition 1. In particular, when SNR$\geq$ 5 dB, $M \geq 40$, $L \geq 100$ or SNR$\geq$ 0 dB, $M \geq 50$, $L \geq 200$, the proposed method can achieve source enumeration almost exactly. For simplicity and also for better performance comparison, the number of sources is supposed to be correctly estimated in the subsequent simulations.

In the second simulation, five ID sources are considered to impinge on the adopted ULA with 40 antennas and two different scenarios are considered. Scenario 1: three FF ID sources with parameters $\{\theta_1 = -50°, \sigma_{\theta_1} = 1°\}$, $\{\theta_2 = -30°, \sigma_{\theta_2} = 1°\}$, $\{\theta_3 = 10°, \sigma_{\theta_3} = 1°\}$ and two NF ID sources with parameters $\{\theta_4 = 30°, \sigma_{\theta_4} = 1°, r_4 = 2\lambda, \sigma_{r_4} = 0.0349\lambda\}$, $\{\theta_5 = 50°, \sigma_{\theta_5} = 1°, r_5 = 3\lambda, \sigma_{r_5} = 0.0524\lambda\}$, where all the DOAs are distinct. Scenario 2: the condition is the same as in scenario 1, except that an FF ID source has the same DOA as the NF one (i.e., $\theta = 10°$). Figs. 3(a) and 3(b) show the spatial spectrums of scenario 1, where SNR and the number of snapshots L are fixed at 10 dB and 200, respectively. The search steps along DOA and range regions are set to $1°$ and $\lambda/30$, respectively. We can see that the proposed method

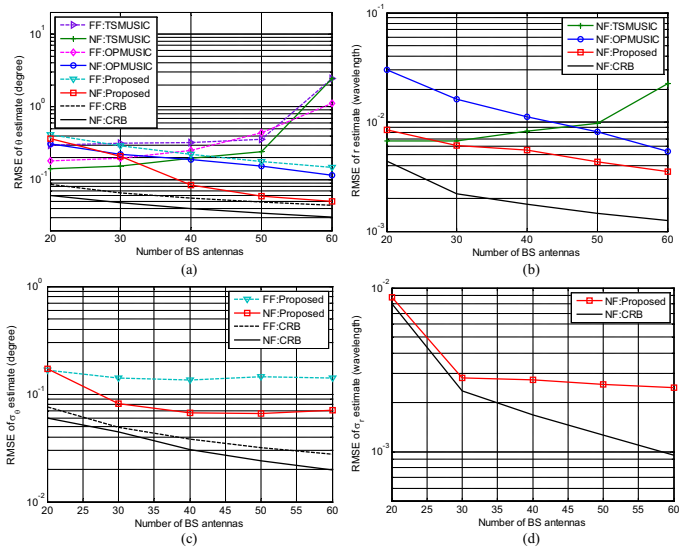

Fig. 4. RMSEs of multi-parameter estimates versus number of BS antennas for one FF and one NF ID sources with $\{\theta_1 = 10^\circ, \sigma_{\theta_1} = 2^\circ\}$, $\{\theta_2 = 30^\circ, \sigma_{\theta_2} = 1^\circ, r_2 = 2\lambda, \sigma_{r_2} = r_2 \cdot \tan(\sigma_{\theta_2})\}$, SNR=10 dB, $L = 200$. (a), (b), (c), and (d) correspond to the estimation of nominal DOA, nominal range, angular spread and range spread, respectively.

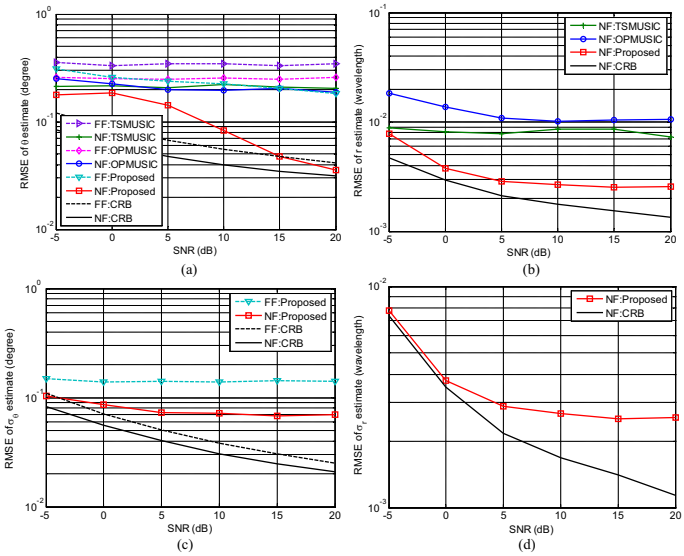

Fig. 5. RMSEs of multi-parameter estimates versus average received SNR for one FF and one NF ID sources with $\{\theta_1 = 10^\circ, \sigma_{\theta_1} = 2^\circ\}$, $\{\theta_2 = 30^\circ, \sigma_{\theta_2} = 1^\circ, r_2 = 2\lambda, \sigma_{r_2} = r_2 \cdot \tan(\sigma_{\theta_2})\}$, M=40, $L = 200$. (a), (b), (c), and (d) correspond to the estimation of nominal DOA, nominal range, angular spread and range spread, respectively.

provides a good source localization result and can distinguish mixed FF and NF ID sources effectively. Figs. 3(c) and 3(d) further shows the spatial spectrums of scenario 2, and it can be clearly observed that the proposed method still works when FF and NF sources have the same DOA.

In the third simulation, we evaluate the performance of the proposed method for different number of antennas M. One FF and one NF ID sources with same parameters as in the first simulation are considered, SNR=10 dB and $L = 200$. The search steps along DOA and range regions are set to 0.1° and $\lambda/600$, respectively. The RMSEs of estimated parameters

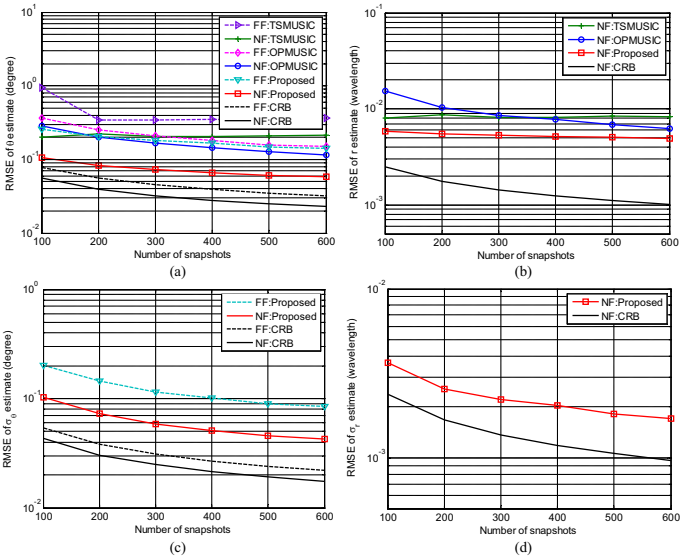

Fig. 6. RMSEs of multi-parameter estimates versus number of snapshots for one FF and one NF ID sources with $\{\theta_1 = 10^\circ, \sigma_{\theta_1} = 2^\circ\}$, $\{\theta_2 = 30^\circ, \sigma_{\theta_2} = 1^\circ, r_2 = 2\lambda, \sigma_{r_2} = r_2 \cdot \tan(\sigma_{\theta_2})\}$, SNR=10 dB, $M = 40$. (a), (b), (c), and (d) correspond to the estimation of nominal DOA, nominal range, angular spread and range spread, respectively.

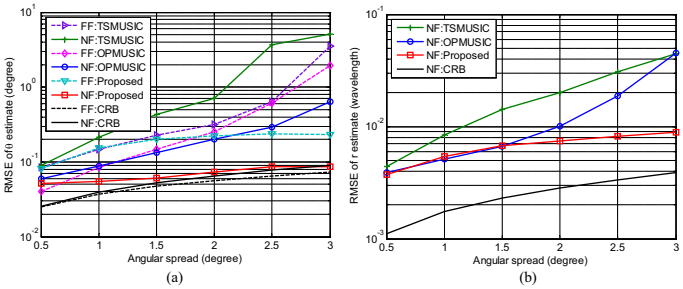

Fig. 7. RMSEs of nominal DOA and nominal range estimates versus angular spread for one FF and one NF ID sources with $\{\theta_1 = 10^\circ\}$, $\{\theta_2 = 30^\circ, r_2 = 2\lambda\}$, $\sigma_{\theta_1} = \sigma_{\theta_2}$, $\sigma_{r_2} = r_2 \cdot \tan(\sigma_{\theta_2})$, $M = 40$, $L = 200$, SNR=10 dB. (a) and (b) correspond to the estimation of nominal DOA and nominal range, respectively.

versus M are plotted in Fig. 4. It can be observed that the RMSEs for nominal DOA and nominal range estimations by the proposed method decrease as M increases. In contrast, the performance of FF nominal DOA estimation of the compared methods degrades with the increase of M due to influence of angular spread, and such an influence increases as M increases for FF nominal DOA estimation. As a result, the FF estimator of both the TSMUSIC method and the OPMUSIC method cannot find the correct signal and noise subspaces under the ID source model. Different from the FF estimator, due to employment of the oblique projection technique and the usage of only part of the covariance matrix, the influence of angular spread on the performance of the NF estimator of the OPMUSIC method is reduced, and hence the NF estimator of the OPMUSIC method performs better than the FF estimator. In addition, since the TSMUSIC method does not apply the oblique projection technique, and the working mechanism of its NF estimator is also different from that of the OPMUSIC, the performance of its NF estimator deteriorates with the

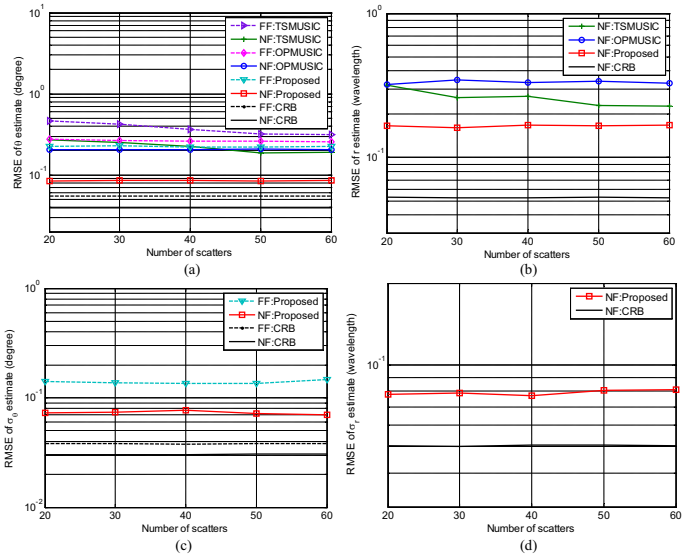

Fig. 8. RMSEs of multi-parameter estimates versus number of scatters for one FF and one NF ID sources with $\{\theta_1 = 10°, \sigma_{\theta_1} = 2°\}$, $\{\theta_2 = 30°, \sigma_{\theta_2} = 1°, r_2 = 2\lambda, \sigma_{r_2} = r_2 \cdot \tan(\sigma_{\theta_2})\}$, SNR=10 dB, $M = 40$, $L = 200$. (a), (b), (c), and (d) correspond to the estimation of nominal DOA, nominal range, angular spread and range spread, respectively.

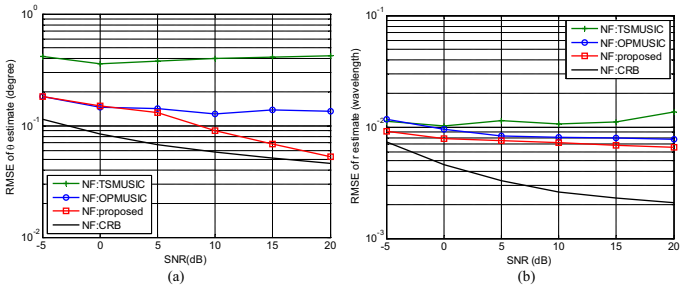

Fig. 9. RMSEs of nominal DOA and nominal range estimates versus average received SNR for two pure NF ID sources with $\{\theta_1 = 10°, \sigma_{\theta_1} = 2°, r_1 = 2\lambda\}, \{\theta_2 = 30°, \sigma_{\theta_2} = 1°, r_2 = 3\lambda\}$, $\sigma_{r_i} = r_i \cdot \tan(\sigma_{\theta_i}), i = 1, 2$, $M = 40$ and $L = 200$. (a) and (b) correspond to the estimation of nominal DOA and nominal range, respectively.

increase of M. On the other hand, it can also be seen that there are clear gaps between the RMSEs of the proposed method and the related CRBs, which is consistent with the analysis in Section IV.

In the fourth simulation, we examine the performance of the proposed method with respect to the average received SNR. M and L are fixed at 40 and 200, respectively. The location information of DTs/ID sources and the search steps along DOA and range regions are the same as those in the third simulation. Figs. 5(a)-5(d) show the RMSEs of different parameter estimates at different SNRs. It can be seen that the RMSEs decrease as SNR increases for the proposed method. In terms of specific metrics, the proposed method outperforms the compared methods when SNR > 0 dB for nominal DOA estimation of the FF ID source; while for other parameters, the proposed method provides a leading performance in the whole SNR region. Moreover, due to the fact that the angular spread of FF ID source is larger than that of NF one, there is a larger gap between the RMSE of nominal DOA estimation of FF ID sources and the CRB, compared with that of other parameters. In addition, it can be found that because of the inconsistent estimation of nominal DOA and nominal range, the gap between spread parameters (including angular spread and range spread) and their corresponding CRBs becomes large as SNR increases.

In the fifth simulation, the performance of the proposed method is studied for different numbers of snapshots. The simulation result is shown in Fig. 6, where SNR=10 dB, M=40 and the number of snapshots varies from 100 to 600 with a step of 100. From the simulation result, it can be seen that the RMSEs of all parameters of the proposed method decrease monotonically with the number of snapshots, and again, the proposed method outperforms the compared ones.

In the sixth simulation, the effect of angular spread on the performance of nominal DOA and nominal range estimations is examined. The configuration of nominal locations of two ID sources are the same as the third to the fifth simulations, and the angular spreads $\sigma_{\theta_1} = \sigma_{\theta_2}$ are changed from $0.5°$ to $3°$, and $\sigma_{r_2} = r_2 \cdot \tan(\sigma_{\theta_2})$. The RMSE curves are shown in Fig. 7 with $M = 40$, $L = 200$ and SNR=10 dB. As can be seen in Fig. 7, the performance of all the considered methods is affected by the angular spread. The difference is that the performance of the proposed method gets worse slightly, while that of the TSMUSIC and OPMUSIC methods degrades rapidly with the increase of angular spread. Notice that the σ_{r_2} increases monotonically with σ_{θ_2}, and hence it can be deduced that their performance will also degrade with the increase of range spread.

In the seventh simulation, the effect of the number of scatters (i.e., the number of multipaths) on the performance is investigated and the RMSE curves are illustrated in Fig. 8. The configuration of nominal locations of two ID sources is again the same as the third to the fifth simulations, except that the number of scatters N_k is varied from 20 to 60, $M = 40$, $L = 200$ and SNR=10 dB. It can be seen that the RMSEs of the proposed method are almost invariant with N_k, which effectively validates the robustness of the proposed method in a multipath environment.

In the last simulation, two pure NF ID sources with their parameters $\{\theta_1 = 10°, \sigma_{\theta_1} = 2°, r_1 = 2\lambda\}, \{\theta_2 = 30°, \sigma_{\theta_2} = 1°, r_2 = 3\lambda\}$, and $\sigma_{r_i} = r_i \cdot \tan(\sigma_{\theta_i}), i = 1, 2$, are considered, $M = 40$, $L = 200$, and SNR varies from -5 dB to 20 dB. The RMSEs for nominal DOA and nominal range estimations are shown in Fig. 9, from which we can see that the proposed method is also suitable for localization of pure NF ID sources. In comparison with the TSMUSIC and OPMUSIC methods, the proposed one can provide improved nominal DOA and nominal range estimation. Moreover, it is necessary to point out here that the proposed method also works for the scenario of pure FF ID sources. When all sources are FF ID ones, the proposed method will reduce to the 1-D RARE estimator proposed in [37]. Since the performance of the 1-D RARE estimator has been fully discussed, this part of the simulation is omitted here.

VI. Conclusion

In this paper, a two-stage RARE based mixed FF and NF ID source localization method has been proposed under the general array manifold model with small angular and range spreads. Firstly, it is verified that AIC combined with DOA estimation results of FF ID sources can achieve source enumeration of real FF and NF sources under a certain condition, and then the shift invariance of FF GAM, the oblique projection and multiple 1-D spectral searches are jointly utilized for localization of mixed FF and NF ID sources. The proposed method can provide an improved localization and source types classification result with reasonable computational complexity. Through performance analysis, approximate CRB derivation as well as numerical simulations, the effectiveness of the proposed method has been demonstrated effectively. As part of our future research, the localization problem of mixed FF and NF distributed sources under an exact spatial propagation geometry will be studied.

Appendix A
Proof of Proposition 1

Define α_k and $\mathbf{v}_k$ as the eigenvalue and eigenvector of $\frac{1}{M}\bar{\mathbf{a}}_k\bar{\mathbf{a}}_k^H$, respectively, where $\bar{\mathbf{a}}_k$ denotes the kth column of $\bar{\mathbf{A}}$, $k \in [1, 3K-K_1]$. Then, we have

$$\bar{P}_k\bar{\mathbf{a}}_k\bar{\mathbf{a}}_k^H = M\bar{P}_k\alpha_k\mathbf{v}_k\mathbf{v}_k^H, \tag{66}$$

which indicates that the eigenvalues of signal components are proportional to the signal power.

According to the general asymptotic theory or the asymptotic behaviour of the sample eigenvalues under the condition of $M, L \to \infty$, and $c = M/L \in (0, \infty)$, the separable condition of the minimum eigenvalue λ_{min} of signal components and the eigenvalue of noise components should satisfy [39], [40]

$$\lambda_{\min} > \sigma_n^2\sqrt{c}. \tag{67}$$

When $\lambda_{\min} \le \sigma_n^2\sqrt{c}$, the existing information theory criterion based source enumeration methods (including the AIC, the Bayesian Information Criterion (BIC), etc.) cannot detect all incident signals [41], [42].

Following (67) and further considering the fact that $\bar{\mathbf{A}}\overline{\mathbf{\Lambda}}\bar{\mathbf{A}} = \sum_{k=1}^{3K-K_1}\overline{\mathbf{\Lambda}}(k,k)\bar{\mathbf{a}}_k\bar{\mathbf{a}}_k^H$, it can be derived that

$$M \cdot \min\{\alpha_k \cdot \overline{\mathbf{\Lambda}}(k,k) | k = 1, \ldots, 3K-K_1\} > \sigma_n^2\sqrt{c}. \tag{68}$$

Notice that small angular and range spreads are assumed in this paper, (68) can be relaxed as

$$M \cdot \min\{P_k\sigma_{\gamma_k}^2\alpha_k | k = 1, \ldots, K\} \cdot \min\{\sigma_{\theta_k}^2, \sigma_{r_k}^2 | k = 1, \ldots, K\} > \sigma_n^2\sqrt{c}. \tag{69}$$

Defining SNR=$10\log_{10}(P_k/\sigma_n^2)$, $\sigma_{\gamma,\alpha}^2 = \min\{\sigma_{\gamma_k}^2\alpha_k | k = 1, \ldots, K\}$ and $\sigma_{\theta,r}^2 = \min\{\sigma_{\theta_k}^2, \sigma_{r_k}^2 | k = 1, \ldots, K\}$, we have

$$10^{\mathrm{SNR}/10} \cdot \sigma_{\gamma,\alpha}^2 \cdot \sigma_{\theta,r}^2 > \frac{1}{\sqrt{ML}}. \tag{70}$$

It can be seen from (24) that distinguishing eigenvalues of signal and noise components plays a fundamental role for the effectiveness of the AIC. That is, the AIC can achieve virtual source enumeration effectively, provided that at least (70) holds. This ends the proof for Proposition 1. □

Appendix B
Derivation of the Approximate CRB

For convenience, we reformulate the approximated array covariance matrix $\mathbf{R}$ as [43]

$$\mathbf{R} \approx \sum_{k=1}^{K_1}\rho_k\mathbf{R}_{sf}(\theta_k, \sigma_{\theta_k}) + \sum_{k=K_1+1}^{K}\rho_k\mathbf{R}_{sn}(\theta_k, r_k, \sigma_{\theta_k}, \sigma_{r_k}) + \sigma_n^2\mathbf{I}_M, \tag{71}$$

where

$$\mathbf{R}_{sf}(\theta_k, \sigma_{\theta_k}) = \mathbf{a}(\theta_k)\mathbf{a}^H(\theta_k) \odot \mathbf{G}_F(\theta_k, \sigma_{\theta_k}), \tag{72}$$

$$\mathbf{R}_{sn}(\theta_k, r_k, \sigma_{\theta_k}, \sigma_{r_K}) = \mathbf{a}(\theta_k, r_k)\mathbf{a}^H(\theta_k, r_k) \odot \mathbf{G}_N(\theta_k, r_k, \sigma_{\theta_k}, \sigma_{r_k}), \tag{73}$$

$\mathbf{G}_F(\theta_k, \sigma_{\theta_k})$ and $\mathbf{G}_N(\theta_k, r_k, \sigma_{\theta_k}, \sigma_{r_k})$ are matrices, whose $(\bar{p}, \bar{q})$th elements are given by

$$[\mathbf{G}_F(\theta_k, \sigma_{\theta_k})]_{\bar{p},\bar{q}} = \exp\left\{-\frac{((p-q)\varpi_k\sigma_{\theta_k})^2}{2}\right\}, \tag{74}$$

$$[\mathbf{G}_N(\theta_k, r_k, \sigma_{\theta_k}, \sigma_{r_k})]_{\bar{p},\bar{q}} = \exp\left\{-\frac{((q-p)\varpi_k + (p^2-q^2)\psi_k)^2\sigma_{\theta_k}^2}{2} - \frac{((p^2-q^2)\phi_k/r_k)^2\sigma_{r_k}^2}{2}\right\}, \tag{75}$$

respectively, where $\bar{p} = p + M/2 + 1/2$, $\bar{q} = q + M/2 + 1/2$, and $p, q \in [\frac{1-M}{2}, \frac{M-1}{2}]$. Note that both angular and range distributions are considered to be Gaussian. $\mathbf{G}_F(\theta_k, \sigma_{\theta_k})$ has been given in literature, while the detailed derivation of $\mathbf{G}_N(\theta_k, r_k, \sigma_{\theta_k}, \sigma_{r_k})$ is given in Appendix C.

The CRB of $\boldsymbol{\xi}$ can be calculated by

$$\mathrm{CRB}(\boldsymbol{\xi}) = \frac{1}{L}\left[\left(\frac{\partial\mathbf{r}}{\partial\boldsymbol{\xi}^T}\right)^H(\mathbf{R}^{-T}\otimes\mathbf{R}^{-1})\frac{\partial\mathbf{r}}{\partial\boldsymbol{\xi}^T}\right]^{-1}, \tag{76}$$

where L is the number of snapshots,

$$\mathbf{r} = \mathrm{vec}(\mathbf{R}) = \mathbf{r}_f + \mathbf{r}_n + \sigma_n^2\mathrm{vec}(\mathbf{I}_M), \tag{77}$$

and

$$\mathbf{r}_f = \sum_{k=1}^{K_1}[\rho_k\mathbf{a}^*(\theta_k)\otimes\mathbf{a}(\theta_k)] \odot \mathrm{vec}(\mathbf{G}_F(\theta_k, \sigma_{\theta_k})), \tag{78}$$

$$\mathbf{r}_n = \sum_{k=K_1+1}^{K}[\rho_k\mathbf{a}^*(\theta_k, r_k)\otimes\mathbf{a}(\theta_k, r_k)] \odot \mathrm{vec}(\mathbf{G}_N(\theta_k, r_k, \sigma_{\theta_k}, \sigma_{r_k})). \tag{79}$$

After partitioning, we have

$$(\mathbf{R}^{-T/2}\otimes\mathbf{R}^{-1/2})\left[\begin{array}{cc}\frac{\partial\mathbf{r}}{\partial\boldsymbol{\mu}^T} & \frac{\partial\mathbf{r}}{\partial\boldsymbol{\nu}^T}\end{array}\right]\overset{def}{=}[\mathbf{W}\quad\mathbf{V}], \tag{80}$$

with the mth column of $\mathbf{W}$ and $\mathbf{V}$ expressed as

$$[\mathbf{W}(:,m)]_{m=1}^{K_1}=\mathbf{F}\frac{\partial\mathbf{r}_f}{\partial\theta_k},k=1,\ldots,K_1,$$

$$[\mathbf{W}(:,m)]_{m=K_1+1}^{K}=\mathbf{F}\frac{\partial\mathbf{r}_n}{\partial\theta_k},k=K_1+1,\ldots,K,$$

$$[\mathbf{W}(:,m)]_{m=K+1}^{2K-K_1}=\mathbf{F}\frac{\partial\mathbf{r}_n}{\partial r_k},k=K_1+1,\ldots,K,$$

$$[\mathbf{W}(:,m)]_{m=2K-K_1+1}^{2K}=\mathbf{F}\frac{\partial\mathbf{r}_f}{\partial\sigma_k},k=1,\ldots,K_1,$$

$$[\mathbf{W}(:,m)]_{m=2K-K_1+1}^{3K-K_1}=\mathbf{F}\frac{\partial\mathbf{r}_n}{\partial\sigma_k},k=K_1+1,\ldots,K,$$

$$[\mathbf{W}(:,m)]_{m=3K-K_1+1}^{4K-2K_1}=\mathbf{F}\frac{\partial\mathbf{r}_n}{\partial\varepsilon_k},k=K_1+1,\ldots,K,$$

$$[\mathbf{V}(:,m)]_{m=1}^{K}=\mathbf{F}\mathrm{vec}(\mathbf{I}_M),$$

$$[\mathbf{V}(:,m)]_{m=K+1}^{2K}=\mathrm{vec}(\mathbf{R}^{-1}).$$

respectively, where $\mathbf{F}=\mathbf{R}^{-T/2}\otimes\mathbf{R}^{-1/2}$.

Then, we can rewrite (76) as

$$\mathrm{CRB}^{-1}(\boldsymbol{\xi})=L\left[\begin{array}{cc}\mathbf{W}^H\mathbf{W} & \mathbf{W}^H\mathbf{V}\\ \mathbf{V}^H\mathbf{W} & \mathbf{V}^H\mathbf{V}\end{array}\right]. \tag{81}$$

As a result, the CRB concerning the parameters of interest is given by

$$\mathrm{CRB}(\boldsymbol{\mu})=\frac{1}{L}\left[\mathbf{W}^H\boldsymbol{\Pi}_V^{\perp}\mathbf{W}\right]^{-1}, \tag{82}$$

where $\boldsymbol{\Pi}_V^{\perp}=\mathbf{I}-\mathbf{V}(\mathbf{V}^H\mathbf{V})^{-1}\mathbf{V}^H$. □

APPENDIX C
DERIVATION OF $\mathbf{G}_N(\theta_k,r_k,\sigma_{\theta_k},\sigma_{r_k})$

Under the condition of large N_k, and small angular and range spreads, the NF ID source covariance matrix can be described as

$$\mathbf{R}_{sn}=\int\int\mathbf{a}(\theta_k+\tilde{\theta},r_k+\tilde{r})\mathbf{a}^H(\theta_k+\tilde{\theta},r_k+\tilde{r})\cdot p_k(\theta;\theta_k,\sigma_{\theta_k})p_k(r;r_k,\sigma_{r_k})d\tilde{\theta}d\tilde{r}, \tag{83}$$

where $p_k(\theta;\theta_k,\sigma_{\theta_k})$ and $p_k(r;r_k,\sigma_{r_k})$ denote the angular and range auto-correlation kernels of the kth NF sources, respectively.

The first-order Taylor approximations of

$$\sin(\theta_k+\tilde{\theta})\approx\sin\theta_k+\tilde{\theta}\cos\theta_k \tag{84}$$

and

$$\frac{\pi}{\lambda(r_k+\tilde{r})}\cos^2(\theta_k+\tilde{\theta})\approx\frac{\pi}{\lambda r_k}\cos^2\theta_k-\tilde{\theta}\frac{\pi}{\lambda r_k}\sin 2\theta_k-\tilde{r}\frac{\pi}{\lambda r_k^2}\cos^2\theta_k \tag{85}$$

reveal that the $(\bar{p},\bar{q})$th element of $\mathbf{R}_{sn}$ can be written as

$$\begin{aligned}[\mathbf{R}_{sn}]_{\bar{p},\bar{q}}=&\int\int e^{-j\frac{2\pi d}{\lambda}(p-q)\sin(\theta_k+\tilde{\theta})+j\frac{\pi d^2}{\lambda(r_k+\tilde{r})}(p^2-q^2)\cos^2(\theta_k+\tilde{\theta})}\\&\cdot p_k(\theta;\theta_k,\sigma_{\theta_k})p_k(r;r_k,\sigma_{r_k})d\tilde{\theta}d\tilde{r}\\\approx&\, e^{-j\frac{2\pi d}{\lambda}(p-q)\sin(\theta_k)+j\frac{\pi d^2}{\lambda r_k}(p^2-q^2)\cos^2\theta_k}\\&\cdot\int e^{j[(p-q)\varpi_k-(p^2-q^2)\psi_k]\tilde{\theta}}p_k(\theta;\theta_k,\sigma_{\theta_k})d\tilde{\theta}\\&\cdot\int e^{-j(p^2-q^2)\phi_k\tilde{r}/r_k}p_k(r;r_k,\sigma_{r_k})d\tilde{r},\end{aligned} \tag{86}$$

where $\bar{p}=p+M/2+1/2,\bar{q}=q+M/2+1/2$, and $p,q\in[\frac{1-M}{2},\frac{M-1}{2}]$.

Notice that the angular and range spreads are assumed to be Gaussian distributed, and hence $[\mathbf{R}_{sn}]_{\bar{p},\bar{q}}$ can be rewritten as

$$\begin{aligned}[\mathbf{R}_{sn}]_{\bar{p},\bar{q}}&=[\bar{\mathbf{A}}(\theta_k,r_k)]_{\bar{p},\bar{q}}\cdot[\mathbf{G}_{N\theta}]_{\bar{p},\bar{q}}\cdot[\mathbf{G}_{Nr}]_{\bar{p},\bar{q}}\\&=[\bar{\mathbf{A}}(\theta_k,r_k)]_{\bar{p},\bar{q}}\cdot[\mathbf{G}_N(\theta_k,r_k,\sigma_{\theta_k},\sigma_{r_k})]_{\bar{p},\bar{q}},\end{aligned} \tag{87}$$

where

$$\bar{\mathbf{A}}(\theta_k,r_k)=\mathbf{a}(\theta_k,r_k)\mathbf{a}^H(\theta_k,r_k), \tag{88}$$

$$[\mathbf{G}_{N\theta}]_{\bar{p},\bar{q}}=\int e^{j[(p-q)\varpi_k-(p^2-q^2)\psi_k]\tilde{\theta}}\frac{1}{\sqrt{2\pi}\sigma_{\theta_k}}e^{\frac{-\tilde{\theta}^2}{2\sigma_{\theta_k}^2}}d\tilde{\theta}, \tag{89}$$

$$[\mathbf{G}_{Nr}]_{\bar{p},\bar{q}}=\int e^{-j(p^2-q^2)\phi_k\tilde{r}/r_k}\frac{1}{\sqrt{2\pi}\sigma_{r_k}}e^{\frac{-\tilde{r}^2}{2\sigma_{r_k}^2}}d\tilde{r}. \tag{90}$$

For a Gaussian function $f(t)=\frac{1}{\sqrt{2\pi}\sigma}e^{-\frac{t^2}{2\sigma^2}}=be^{-at^2}$, the following transformation holds

$$\begin{aligned}F(\varsigma)=&\int f(t)e^{-j\varsigma t}dt=\int be^{-at^2}e^{-j\varsigma t}dt\\=&\,b\int e^{-(at^2+j\varsigma t)}dt=b\int e^{-a(t+\frac{j\varsigma}{2a})^2-\frac{\varsigma^2}{4a}}dt\\=&\,be^{-\frac{\varsigma^2}{4a}}\int e^{-(\sqrt{a}t+\frac{j\varsigma}{2\sqrt{a}})^2}dt\\\overset{u=\sqrt{a}t+\frac{j\varsigma}{2\sqrt{a}}}{=\!=\!=}&\,\frac{b}{\sqrt{a}}e^{-\frac{\varsigma^2}{4a}}\int e^{-u^2}du=b\sqrt{\frac{\pi}{a}}e^{-\frac{\varsigma^2}{4a}}\\=&\,e^{\frac{-\varsigma^2\sigma^2}{2}},\end{aligned} \tag{91}$$

which directly yields

$$[\mathbf{G}_{N\theta}]_{\bar{p},\bar{q}}=\exp\left\{-\frac{((q-p)\varpi_k+(p^2-q^2)\psi_k)^2\sigma_{\theta_k}^2}{2}\right\}, \tag{92}$$

$$[\mathbf{G}_{Nr}]_{\bar{p},\bar{q}}=\exp\left\{-\frac{((p^2-q^2)\phi_k/r_k)^2\sigma_{r_k}^2}{2}\right\}. \tag{93}$$

Finally, it can be derived that the expression of $\mathbf{G}_N(\theta_k,r_k,\sigma_k,\varepsilon_k)$ is given by Eq. (75). □

REFERENCES

[1] R. Wu, M. Wang, and Z. Zhang, "Computationally efficient DOA and carrier estimation for coherent signal using single snapshot and its time-delay relications," *IEEE Trans. Aerosp. Electron. Syst*., vol. 57, no. 4, pp. 2469-2480, Aug. 2021.

[2] H. Xiang, B. Chen, and M. Yang, "Angle separation learning for coherent DOA estimation with deep sparse prior," *IEEE Commun. Lett*., vol. 25, no. 2, pp. 465-469, Feb. 2021.

[3] G. P. Blasone, F. Colone, P. Lombardo, P. Wojaczek, and D. Cristallini, "Passive radar stap detection and DOA estimation uder antenna calibration errors," *IEEE Trans. Aerosp. Electron. Syst*., vol. 57, no. 5, pp. 2725-2742, Oct. 2021.

[4] R. C. Johnson, Antenna Engineering Handbook, 3rd ed. New York: McGraw-Hill, pp. 9-12, 1993.

[5] Y. Tian, J. Shi, H. Yue, and X. Rong, "Calibrating nested sensor arrays for DOA estimation utilizing continuous multiplication operator," *Signal Process*., vol. 176, pp. 107674, 2020.

[6] H. Chen, W. Wang, and W. Liu, "Augmented quaternion ESPRIT-type DOA estimation with a crossed-dipole array," *IEEE Commun. Lett*., vol. 24, no. 3, pp. 548-552, Mar. 2020.

[7] W. Zuo, J. Xin, N. Zheng, H. Ohmori, and A. Sano, "Subspace-based near-field source localization in unknown spatially nonuniform noise environment," *IEEE Trans. Signal Process*., vol. 68, pp. 4713-4726, Aug. 2020.

[8] Y. Fang, S. Zhu, Y. Gao, and C. Zeng, "DOA estimation for coherent signals with improved sparse representation in the presence of unknown spatially correlated Gaussian noise," *IEEE Trans. Veh. Technol*., vol. 69, no. 9, pp. 10059-10069, Sept. 2020.

[9] D. Malioutov, M. Cetin, and A. S. Willsky, "A sparse signal reconstruction perspective for source localization with sensor arrays," *IEEE Trans. Signal Process*., vol. 53, vol. 8, pp. 3010-3022, Aug. 2005.

[10] H. Liu, H. Meng, L. Gan, D. Li, Y. Zhou, and T. K. Truong, "Subspace and sparse reconstruction based near-field sources localization in uniform linear array," *Digital Signal Process*., vol. 106, pp. 102824, Nov. 2020.

[11] H. Huang, J. Yang, H. Huang, et al., "Deep learning for super-Resolution channel estimation and DOA estimation based massive MIMO system," *IEEE Trans. Veh. Technol*., vol. 67, no. 9, pp. 8549-8560, Sept. 2018.

[12] L. Wan, Y. Sun, L. Sun, Z. Ning, and Joel J. P. C. Rodrigues, "Deep learning based autonomous vehicle super resolution DOA estimation for safety driving," *IEEE Trans. Intell. Transp. Syst*., vol. 22, no. 7, Jul. 2021.

[13] K. Zheng, S. Ou, and X. Yin, "Massive MIMO channel models: A survey," *Int. J. Antennas Propag*., vol. 2014, Article ID 848071.

[14] J. He, L. Li, T. Shu, and T. K. Truong, "Mixed near-field and far-field source localization based on exact spatial propagation geometry," *IEEE Trans. Veh. Technol*., vol. 70, no. 4, pp. 3540-3551, Apr. 2021.

[15] J. Liang and D. Liu, "Passive localization of mixed near-field and far-field sources using two-stage MUSIC algorithm," *IEEE Trans. Signal Process*., vol. 58, vol. 1, pp. 108-120, Jan. 2010.

[16] J. He, M. N. S. Swany, and M. O. Ahmad, "Efficient application of music algorithm under the coexistence of far-field and near-field sources," *IEEE Trans. Signal Process*., vol. 60, no. 4, pp. 2066-2070, Apr. 2012.

[17] G. Liu and X. Sun, "Spatial differencing method for mixed far-field and near-field sources localization," *IEEE Signal Process. Lett*., vol. 21, no. 11, pp. 1331-1335, Nov. 2014.

[18] X. Wu and J. Yan, "3-D mixed far-field and near-field sources localization with cross array," *IEEE Trans. Veh. Technol*., vol. 69, no. 6, pp. 6833-6837, Jun. 2020.

[19] Z. Zheng, M. Fu, W. Wang, S. Zhang, and Y. Liao, "Localization of mixed near-field and far-field sources using symmetric double-nested arrays," *IEEE Trans. Antennas Propag*., vol. 67, no. 11, pp. 7059-7070, Nov. 2019.

[20] Z. Zheng, M. Fu, W. Wang, and H. C. So, "Symmetric displaced coprime array configurations for mixed near- and far-field source localization," *IEEE Trans. Antennas Propag*., vol. 69, no. 1, pp. 465C477, Jan. 2021.

[21] Y. Tian, Q. Lian, and H. Xu, "Mixed near-field and far-field source localization utilizing symmetric nested array," *Digital Signal Process*., vol. 73, pp. 16-23, 2018.

[22] H. Chen, W. Liu, W. Zhu, and M. N. S. Swamy, "Noncircularity-based localization for mixed near-field and far-field sources with unknown mutual coupling," in *Proc. IEEE Int. Conf. Acoust., Speech, Signal Process*., Calgary, Alberta, Canada, 2018, pp. 3236-3240.

[23] R. Raich, J. Goldberg, and H. Messer, "Bearing estimation for a distributed source: Modeling, inherent accuracy limitations and algorithms," *IEEE Trans. Signal Process*., vol. 48, no. 2, pp. 429-441, Feb. 2000.

[24] S. Valaee, B. Champagne, and P. Kabal, "Parametric localization of distributed sources," *IEEE Trans. Signal Process*., vol. 43, no. 9, pp. 2144-2153, Sept. 1995.

[25] L. Wan, G. Han, J. Jiang, *et al.*, "DOA estimation for coherently distributed sources considering circular and noncircular signals in massive MIMO systems," *IEEE Syst. J.*, vol. 11, no. 1, pp. 41-49, Mar. 2017.

[26] Y. Liu, L. Hou, Q. Shen, *et al.*, "Beamspace U-ESPRIT DOA estimation algorithm of coherently distributed sources in massive MIMO systems," in *Proc. Advanced Computational Intell*., Dali, China, Aug. 2020, pp. 126-132.

[27] H. Xu, Y. Tian, and S. Liu, "Linear-shrinkage-based DOA estimation for coherently distributed sources considering mutual coupling in massive MIMO systems," *Int. J. Electron. Commun*., vol. 126, pp. 153398, 2020.

[28] Y. Tian, H. Yue, and X. Rong, "Multi-parameters estimation of coherently distributed sources under coexistence of circular and noncircular signals," *IEEE Commun. Lett*., vol. 24, no. 6, pp. 1254-1257, Jun. 2020.

[29] Y. Meng, P. Stoica, and K. Wong, "Estimation of the directions of arrival of spatially dispersed signals in array processing," in *Proc. IEE Radar, Sonar Navigat*., vol. 143, no. 1, pp. 1-9, Feb. 1996.

[30] A. Hu, T. Lv, H. Cao, *et al.*, "An ESPRIT-based approach for 2-D localization of incoherenltly distributed sources in massive MIMO systems," *IEEE J. Sel. Topics Signal Process.*, vol. 8, no. 5, pp. 996-1011, Oct. 2014.

[31] Y. Tian, W. Liu, H. Xu, S. Liu, and Z. Dong, "2-D DOA estimation of incoherently distributed sources considering gain-phase perturbations in massive MIMO systems," *IEEE Trans. Wireless Commun*., vol. 21, no. 2, pp. 1143-1155, Feb. 2022.

[32] Z. Zheng, W. Wang, H. Meng, *et al.*, "Efficient beanspace-based algorithm for two-dimensional DOA estimation of incoherently distributed sources in massive MIMO systems," *IEEE Trans. Veh. Technol*., vol. 67, no. 12, pp. 11776-11789, Dec. 2018.

[33] H. Boujemaa, "Extension of COMET algorithm to multiple diffuse source localization in zaimuth and elevation," *Eur. Trans. Telecommun*., vol. 16, no. 6, pp. 557-566, Nov./Dec. 2005.

[34] L. Yang, J. Li, F. Chen, Y. Wei, F. Ji, and H. Yu, "Joint angular-frequency distribution estimation of incoherently distributed wideband sources via low-rank matrix recovery," *IEEE Trans. Aerosp. Electron. Syst*., vol. 57, no. 6, pp. 3563-3573, Dec. 2021.

[35] J. A. Chaaya, J. Picheral, and S. Marcos, "Localization of spatially distributed near-field sources with unknown angular spread shape," *Signal Process*., vol. 106, pp. 259-265, 2015.

[36] L. Yang, J. Li, F. Chen, Y. Wei, F. Ji, and H. Yu, "Localization of incoherently distributed near-field sources: A low-rank matrix recovery approach," *Signal Process*., vol. 189, pp. 108273, 2021.

[37] R. Cao, F. Gao, and X. Zhang, "An angular parameter estimation method for incoherently distributed sources via generalized shift invariance," *IEEE Trans. Signal. Process*., vol. 64, no.17, pp. 4493-4503, 2016.

[38] R. Boyer and G. Bouleux, "Oblique projections for direction-of-arrival estimation with prior knowledge," *IEEE Trans. Signal Process*., vol. 56, no. 4, pp. 1374-1387, Apr. 2008.

[39] B. A. Johnson, Y. I. Abramovich, and X. Mestre, "MUSIC, G-MUISC, and maximum-likelihood performance breakdown," *IEEE Trans. Signal. Process*., vol. 56, no.8, pp. 3944-3958, Aug. 2008.

[40] P. Vallet, X. Mestre, and P. Loubaton, "Performance analysis of an improved MUSIC DOA estimator," *IEEE Trans. Signal. Process*., vol. 63, no.23, pp. 6407-6422, Dec. 2015.

[41] R. R. Nadakuditi and A. Edelman, "Sample eigenvalue based detection of high-dimensional signals in white noise using relatively few samples," *IEEE Trans. Signal. Process*., vol. 56, no. 7, pp. 2625-2638, Jul. 2008.

[42] L. Huang, Y. Xiao, K. Liu, H. C. So, and J. -K. Zhang, "Bayesian information criterion for source enumeration in large-scale adaptive antenna array," *IEEE Trans. Veh. Technol*., vol. 65, no. 5, pp. 3018-3032, May 2016.

[43] W. J. Bangs, "Array processing with generalized beamformers," Ph. D. dissertation, Yale Univ., New Haven, CT, USA, 1971.

Ye Tian (Member, IEEE) received the B.S. and Ph.D. degrees from the College of Communication Engineering, Jilin University, Changchun, China, in 2009 and 2014, respectively. He won a Huawei scholarship in 2013 and was selected as a young top talent by the Hebei Provincial Department of Education in 2016. He is currently an Associate Professor in Faculty of Information Science and Engineering, Ningbo University. He has published more than 30 international peer-reviewed journal/conference papers and more than 10 patents. His research interests include array signal processing, autonomous vehicle positioning, massive MIMO as well as large-dimensional random matrix theory.

Xinyu Gao received the B.S. degree from the Yantai University, Yantai, China, in 2015, and the M.Eng degree from the school of information science and engineering, Yanshan University, Qinhuangdao, China, in 2022. Her main research interests include direction-of-arrival estimation, array signal processing and massive MIMO.

Wei Liu (Senior Member, IEEE) received his BSc and LLB. degrees from Peking University, China, in 1996 and 1997, respectively, MPhil from the University of Hong Kong in 2001, and PhD from the School of Electronics and Computer Science, University of Southampton, UK, in 2003. He then worked as a postdoc first at Southampton and later at the Department of Electrical and Electronic Engineering, Imperial College London. Since September 2005, he has been with the Department of Electronic and Electrical Engineering, University of Sheffield, UK, first as a Lecturer and then a Senior Lecturer. He has published about 350 journal and conference papers, five book chapters, and two research monographs titled "Wideband Beamforming: Concepts and Techniques" (John Wiley, March 2010) and "Low-Cost Smart Antennas" (by Wiley-IEEE, March 2019), respectively. His research interests cover a wide range of topics in signal processing, with a focus on sensor array signal processing and its various applications, such as robotics and autonomous systems, human computer interface, radar, sonar, satellite navigation, and wireless communications.

He is a member of the Digital Signal Processing Technical Committee of the IEEE Circuits and Systems Society (Secretary from May 2020) and the Sensor Array and Multichannel Signal Processing Technical Committee of the IEEE Signal Processing Society (Chair from Jan 2021). He was an Associate Editor for IEEE Trans. on Signal Processing (2015-2019) and IEEE Access (2016-2021), and is currently an editorial board member of the journal Frontiers of Information Technology and Electronic Engineering and the Journal of The Franklin Institute.

Hua Chen (Member, IEEE) received the M.Eng. and Ph.D. degrees in Information and Communication Engineering from Tianjin University, Tianjin, China, in 2013 and 2017, respectively. He is currently an Associate Professor in Faculty of Information Science and Engineering, Ningbo University, China. His research interests include array signal processing and MIMO radar.

Dr. Chen is currently an Associated Editor for Circuits, Systems, and Signal Processing.

Gang Wang (Senior Member, IEEE) received the B.Eng. degree from Shandong University, Jinan, China, and the Ph.D. degree from Xidian University, Xian, China, both in electronic engineering, in 2006 and 2011, respectively. He joined Ningbo University, Ningbo, China, in January 2012, where he is currently a full Professor. Form January 2014 to April 2014, he was a Research Associate at the Chinese University of Hong Kong, Hong Kong, China. From June 2018 to June 2019, he was a Visiting Scholar at the University of Missouri, Columbia, USA. His research interests are in the areas of target localization and tracking in wireless networks, array signal processing, and robust ellipse fitting in image processing.

He is the winner of the Distinguished Young Scholars of Zhejiang Provincial Natural Science Foundation and a member of the IEEE Signal Processing Society Sensor Array and Multichannel (SAM) Technical Committee. He currently serves as Handling Editor for Digital Signal Processing (Elsevier) and Signal Processing (Elsevier), and Associate Editor for IEEE Transactions on Aerospace and Electronic Systems.

Yunbai Qin received the B.S. and M.Eng. degrees in communication engineering from Jilin University, Changchun, China, in 2008 and 2011, respectively. He is currently a Lecturer with the School of Electronic Engineering, Guangxi Normal University. His research interests include machine vision, array signal processing, intelligent robot, automotive electronics, and transportation infrastructure big data.